A&A, 711, A40 (2026)
https://doi.org/10.1051/0004-6361/202557391

Astronomy & Astrophysics
Special issue

Euclid Quick Data Release (Q1)

Euclid: Quick Data Release (Q1) – The connection between galaxy close encounters and radio activity⋆

M. Magliocchetti[1,⋆⋆], A. La Marca[2,3], L. Bisigello[4], M. Bondi[5], F. Ricci[6,7], S. Fotopoulou[8], L. Wang[2,3], R. Scaramella[7,9], L. Pentericci[7], I. Prandoni[5], J. G. Sorce[10,11], H. J. A. Rottgering[12], M. J. Hardcastle[13], J. Petley[12], F. La Franca[6,7], K. Rubinur[14], Y. Toba[15,16], Y. Zhong[17,6], M. Mezcua[18,19], G. Zamorani[20], F. Shankar[21], B. Altieri[22], S. Andreon[23], N. Auricchio[20], C. Baccigalupi[24,25,26,27], M. Baldi[28,20,29], S. Bardelli[20], A. Biviano[25,24], E. Branchini[30,31,23], M. Brescia[32,33], J. Brinchmann[34,35,36], S. Camera[37,38,39], G. Cañas-Herrera[40,12], V. Capobianco[39], C. Carbone[41], J. Carretero[42,43], M. Castellano[7], G. Castignani[20], S. Cavuoti[33,44], K. C. Chambers[45], A. Cimatti[46], C. Colodro-Conde[47], G. Congedo[48], C. J. Conselice[49], L. Conversi[50,22], Y. Copin[51], A. Costille[52], F. Courbin[53,54,55], H. M. Courtois[56], M. Cropper[57], A. Da Silva[58,59], H. Degaudenzi[60], G. De Lucia[25], A. M. Di Giorgio[1], H. Dole[11], F. Dubath[60], C. A. J. Duncan[48], X. Dupac[22], S. Dusini[61], S. Escoffier[62], M. Farina[1], R. Farinelli[20], F. Faustini[7,63], S. Ferriol[51], F. Finelli[20,64], M. Frailis[25], E. Franceschi[20], P. Franzetti[41], M. Fumana[41], S. Galeotta[25], K. George[65], B. Gillis[48], C. Giocoli[20,29], J. Gracia-Carpio[66], A. Grazian[4], F. Grupp[66,67], S. V. H. Haugan[14], J. Hoar[22], W. Holmes[68], I. M. Hook[69], F. Hormuth[70], A. Hornstrup[71,72], K. Jahnke[73], M. Jhabvala[74], B. Joachimi[75], E. Keihänen[76], S. Kermiche[62], A. Kiessling[68], B. Kubik[51], M. Kümmel[67], H. Kurki-Suonio[77,78], A. M. C. Le Brun[79], S. Ligori[39], P. B. Lilje[14], V. Lindholm[77,78], I. Lloro[80], G. Mainetti[81], D. Maino[82,41,83], E. Maiorano[20], O. Mansutti[25], O. Marggraf[84], M. Martinelli[7,9], N. Martinet[52], F. Marulli[85,20,29], R. J. Massey[86], E. Medinaceli[20], S. Mei[87,88], Y. Mellier[89,90], M. Meneghetti[20,29], E. Merlin[7], G. Meylan[91], A. Mora[92], M. Moresco[85,20], L. Moscardini[85,20,29], R. Nakajima[84], C. Neissner[93,43], R. C. Nichol[94], S.-M. Niemi[40], C. Padilla[93], S. Paltani[60], F. Pasian[25], K. Pedersen[95], W. J. Percival[96,97,98], V. Pettorino[40], S. Pires[99], G. Polenta[63], M. Poncet[100], L. A. Popa[101], L. Pozzetti[20], F. Raison[66], A. Renzi[102,61], J. Rhodes[68], G. Riccio[33], E. Romelli[25], M. Roncarelli[20], R. Saglia[67,66], Z. Sakr[103,104,105], D. Sapone[106], B. Sartoris[67,25], M. Schirmer[73], P. Schneider[84], T. Schrabback[107], A. Secroun[62], G. Seidel[73], S. Serrano[19,108,18], P. Simon[84], C. Sirignano[102,61], G. Sirri[29], L. Stanco[61], J. Steinwagner[66], P. Tallada-Crespí[42,43], A. N. Taylor[48], I. Tereno[58,109], N. Tessore[75,57], S. Toft[72,110], R. Toledo-Moreo[111], F. Torradeflot[43,42], I. Tutusaus[18,19,104], L. Valenziano[20,64], J. Valiviita[77,78], T. Vassallo[25,65], G. Verdoes Kleijn[3], A. Veropalumbo[23,31,30], Y. Wang[112], J. Weller[67,66], E. Zucca[20], M. Huertas-Company[47,113,114,115], and V. Scottez[89,116]

(Affiliations can be found after the references)

Received 24 September 2025 / Accepted 11 February 2026

ABSTRACT

Using the vast statistics provided by both *Euclid* and the LOFAR surveys, we present the first large-scale study of the connection among radio emission, its morphology, and the merging properties of the hosts of radio sources up to $z \sim 2$. By dividing the radio sample into active galactic nuclei (AGNs) and star-forming galaxies, we find that radio-emitting AGNs show a clear preference for residing within galaxies undergoing a merging event. This is more significant for AGNs that present complex or extended radio emission; indeed, about half of them are associated with merging systems, while only ∼15% are hosted by a non-interacting galaxy. The observed trend is primarily driven by AGNs residing at $z < 1$, especially in the case of high – $P_{144\,\mathrm{MHz}} > 10^{24}\,\mathrm{W\ Hz^{-1}\,sr^{-1}}$ – radio luminosities (∼56% in mergers versus ∼10% in non-mergers regardless of radio appearance). On the other hand, this preference seems to disappear at higher redshifts, where only bright AGNs with extended radio emission still prefer galaxies undergoing a merging event. The situation is reversed in the case of radio-emitting star-forming galaxies, which are preferentially associated with non-interacting systems. This is more significant as we move towards low-radio-luminosity/star-formation objects ($P_{144\,\mathrm{MHz}} < 10^{23}\,\mathrm{W\,Hz^{-1}\,sr^{-1}}$) for which we find ∼40% in non-mergers versus ∼20% in mergers. These values hold regardless of redshift. We interpreted the above result for AGNs with their need to accrete outer gas from local encounters in order to trigger (radio) activity, especially in the case of extended radio emission such as hot spots and lobes. This is mostly observed at $z < 1$, since galaxies in the local Universe are more gas deprived than their higher redshift counterparts. Internal gas reservoirs instead seem sufficient to trigger star formation within the majority of galaxies, which indeed mostly appear as non-interacting systems at all redshifts probed.

Key words. galaxies: active – galaxies: evolution – galaxies: interactions – galaxies: jets – galaxies: nuclei – radio continuum: galaxies

⋆ This paper is published on behalf of the Euclid Consortium.
⋆⋆ Corresponding author: manuela.magliocchetti@inaf.it

1. Introduction

In recent years there has been a rising interest in understanding the possible connection between active galactic nucleus (AGN) activity and close galaxy–galaxy encounters such as merging events. This possibility has mainly been investigated for AGNs selected at optical, X-ray, and mid-IR wavelengths (e.g. Ellison et al. 2019; Pierce et al. 2023; Tanaka et al. 2023; Bickley et al. 2024; La Marca et al. 2024; Euclid Collaboration: La Marca et al. 2026, just to mention few of the most recent works). In general, there seems to be a consensus for a positive link between the two phenomena (i.e. AGN activity being more frequently associated with merging systems), even though some studies claim this to be only confined to mid-IR-selected AGNs, and to be entirely lost in specific galaxy populations such as dwarfs (e.g. Bichang'a et al. 2024; Villforth et al. 2019; Eróstegui et al. 2025; see also Villforth 2023 for a recent review). Other unsolved issues concern possible dependencies of the observed frequency of galaxy mergers in AGN hosts on AGN luminosity (e.g. Comerford et al. 2024), dust obscuration (e.g. Ricci et al. 2021), and/or environment (e.g. Koulouridis et al. 2024).

Even more uncertain is the situation for radio-selected AGNs, which constitute a relatively small fraction of the general AGN population observed at other wavelengths (e.g. Hickox et al. 2009, but see Calistro Rivera et al. 2024 for more recent results based on deeper radio observations), even though their incidence is observed to largely increase with the stellar mass of the host galaxy (e.g. Sabater et al. 2019; Magliocchetti et al. 2020). Indeed, relatively little information can be found in the literature on possible effects of galaxy mergers on radio activity of AGN origin. Moreover, in general the results are hampered by small sample statistics.

Heckman et al. (1986) analysed 43 powerful radio AGNs at $z < 0.3$, finding disturbed optical morphologies which are explainable by galaxy encounters for about 44% of them; this figure decreases (to about 30%) if only limiting to a subsample of 23 radio-luminosity-complete sources. These disturbances were more frequently observed for objects belonging to the Fanaroff–Riley (FR; Fanaroff & Riley 1974) II class with strong emission lines in their optical spectra (high-excitation radio galaxies; HERGs), indicating efficient accretion onto the central black hole. Ramos Almeida et al. (2011) considered 46 radio-bright, $0.05 < z < 0.7$ sources from the 2Jy sample (Tadhunter et al. 1993) – mainly FR II-HERGs – and for this population they reported a merger frequency of about 94%. For the 11 sources showing weak or no emission lines in their optical spectra (low-excitation radio galaxies; LERGs), which is indicative of inefficient accretion, they instead found a value of ∼27%, irrespectively of radio morphology since this latter sample was a mixture of FR Is and FR IIs. Chiaberge et al. (2015) instead presented their analysis for 19 type 2 radio-loud AGNs at $1 < z < 2.5$ spanning five decades in radio power. The 11 objects taken from the 3CR catalogue (Spinrad et al. 1985) were all FR IIs, and they found that all of these were associated with merging events. The same was true for 88% of the eight fainter, radio-loud AGNs considered in the analysis. These results were then compared with lower redshift samples for which the reported merging fraction was ∼70%, making the authors conclude that not only are virtually all radio-loud AGNs associated with merging systems, but also that such a phenomenon is independent of both redshift and radio luminosity.

Results similar to those of Chiaberge et al. (2015) were presented by Breiding et al. (2024) for 28 radio-loud quasars at $1 < z < 2$ from the 3CR catalogue, while, on the other hand, Pierce et al. (2019) found that for a local sample of 30 intermediate radio-luminosity HERGs, the fraction of hosts with merging signatures was ∼53%, which is much lower than what was reported for brighter 2Jy sources by Ramos Almeida et al. (2011) and also dependent on radio luminosity (∼67% versus ∼40% for the brighter versus the fainter half). This luminosity dependence (although more visible in the optical than in the radio band) was more recently confirmed by Pierce et al. (2022) for a larger sample of 155 radio AGNs at $z < 0.3$. Indeed, according to the above work, the fraction of HERGs associated with galaxies that exhibit optical signatures of disturbance goes from 37% to 57% in their radio-brightest sample.

Different findings were recently obtained in the case of LERGs, which – in agreement with the work of Ramos Almeida et al. (2011) – do not seem to show any significant enhancement in the frequency of galaxy close interactions when compared to the general galaxy population (∼27%; e.g. Gordon et al. 2019 and Gao et al. 2020; see also Ellison et al. 2015), at least in the local ($z \simeq 0$) Universe.

Finally, a recent study by Wang et al. (2025) reported an excess of close (<18 kpc) companions around $z \simeq 3.5$ luminous radio-loud AGNs. However, the sample is limited to just four sources.

From the above discussion, it follows that, although there seems to be some convergence in a scenario that envisages a connection between merging events and the triggering of (radio) AGN activity (mainly in the case of efficient gas accretion onto the central black hole that is thought to produce the HERG population; e.g. Hardcastle & Croston 2020), issues still remain, especially regarding the possible dependence of this connection on radio luminosity, radio morphology, or cosmic evolution (i.e. high redshift versus local Universe).

The present paper aims to fill this gap, thanks to the excellent statistical power provided by the LOw-Frequency ARray (LOFAR; van Haarlem et al. 2013) and *Euclid* surveys (Euclid Collaboration: Mellier et al. 2025), which in both cases combine sensitivity with large probed areas. In particular, our analysis is concentrated on 10 $\deg^2$ centred on the so-called Euclid Deep Field North (EDF-N), which are simultaneously covered by deep LOFAR (Bondi et al. 2024) and Euclid Quick Release Q1 (2025) (Q1; Euclid Collaboration: Aussel et al. 2026) observations. Very high-resolution images (mean full width at half maximum of 0.″158, with a standard deviation of 0.″001) captured by the VIS instrument (Euclid Collaboration: Cropper et al. 2025) on board *Euclid* were obtained for all galaxies down to a completeness limit of $I_E = 25.5$ (Euclid Collaboration: McCracken et al. 2026). This allowed the investigation of the morphological properties of *Euclid* galaxies, at least for the bright tail of the distribution (e.g. Euclid Collaboration: Quilley et al. 2026; Euclid Collaboration: Walmsley et al. 2026; Euclid Collaboration: Huertas-Company et al. 2026; Euclid Collaboration: Siudek et al. 2026; Euclid Collaboration: Matamoro Zatarain et al. 2026, Euclid Collaboration: Stevens et al. 2026) and the classification of objects on the basis of their optical appearance as non-interacting or as undergoing a merging event (Euclid Collaboration: La Marca et al. 2026, hereafter EC:LM26).

For the present work, we incorporated the information provided by EC:LM26 into the description of the LOFAR sources presented in Bondi et al. (2024), which were categorised as AGNs and star-forming galaxies (SFGs) following the method

proposed by Magliocchetti et al. (2014). For both populations, we combined radio emission and optical appearance in order to investigate possible links between these two observables. Particular attention will be devoted to those sources that present signatures for complex or extended radio emission such as lobes, jets, or more diffuse patterns.

The paper is structured as follows. In Sect. 2, we introduce the radio catalogue and the method adopted to distinguish between AGNs and SFGs, while in Sect. 3 the *Euclid* sample obtained from VIS observations and the combined catalogue used for the subsequent analysis are outlined. Section 4 presents our results for radio-selected AGNs and SFGs. Here, we also discuss possible systematics in our analysis. Lastly, Sect. 5 features an investigation of our findings in a broader context as well as our conclusions. Some radio and optical cutouts for LOFAR sources with an extended radio morphology are shown in Appendix C. Throughout the paper, we assume a ΛCDM cosmology with $H_0 = 70\,\mathrm{km\,s^{-1}\,Mpc^{-1}}$, $\Omega_\mathrm{m} = 0.3$, and $\Omega_\Lambda = 0.7$.

2. Radio selection

2.1. Radio data

Bondi et al. (2024) presented the first deep (72 hours of observations) radio image of the EDF-N region obtained with the LOFAR High Band Antenna (HBA) at 144 MHz. The observations produced a 6″ resolution image with a central rms noise of $32\,\mu\mathrm{Jy\,beam^{-1}}$. A catalogue of 23 333 radio sources above a signal-to-noise ratio (S/N) threshold of five was extracted from the inner circular $10\,\mathrm{deg^2}$ region. As a result of a visual inspection of the radio morphologies and with the support of deep IRAC images from the unWISE five-year catalogue (Schlafly et al. 2019), radio sources were split into two main categories: those whose radio emission could be fitted by the Python Blob Detector and Source Finder (PyBDSF) with a single Gaussian component, and those that required multiple Gaussian components. In this paper, we refer to the first category as *compact* or *single* (S) radio sources and to the second one as *extended* (E) radio sources. A sub-category of this latter class contains sources whose components were classified by PyBDSF as distinct objects. This can happen when, for example, the lobes of a very extended radio galaxy are separated by tens of arcseconds or even arcminutes. These cases were also all visually investigated in Bondi et al. (2024) with the help of IRAC images, and in the following we refer to them as *complex* radio sources. The category of extended radio sources (including the complex ones) constitutes 7% of the total radio counts.

Bisigello et al. (2025; hereafter B25) provided optical and near-infrared counterparts to the Bondi et al. (2024) radio sources, obtained by following a robust identification strategy that combines the statistical power of the likelihood-ratio (LR; e.g. Sutherland & Saunders 1992) method – including both colour and magnitude information – with targeted visual inspection. After masking regions close to stars and with unreliable photometry in the optical or near-infrared, the final catalogue includes 19 550 radio sources, 19 401 of which (corresponding to a remarkable identification rate of 99.2%) have a reliable counterpart. Photometric redshifts were then derived using optical-to-radio data by following two different methods available from the `CIGALE` (Buat et al. 2018) SED-fitting routine; the first one corresponds to the value of the best spectral-energy-distribution (SED) template (i.e. the one with the minimum χ^2), while the second is derived with a Bayesian-like approach (see Noll et al. 2009 for more details). Although neither of the two methods returns very precise redshift determinations (the fraction of outliers is 18.5% in the first case and 22.8% in the second – cf. B25), these are good enough to provide a redshift distribution for the LOFAR sources in the EDF-N, which is in agreement with the distributions presented by Duncan et al. (2021) for the other three LOFAR deep fields (Boötes, Lockman Hole, and ELAIS-N1); therefore, they are also good enough for the purposes of the present work, which used redshifts only for statistical purposes and – as becomes clearer in the next section – excluded objects with a poor redshift determination. We note that about 20% of the radio sources in the B25 catalogue have a spectroscopic redshift determination from the Dark Energy Spectroscopic Instrument (DESI; DESI Collaboration 2024).

We stress that we preferred to adopt the photometric redshifts presented in B25 with respect to those derived in Euclid Collaboration: Tucci et al. (2026), as the latter analysis does not include IRAC (Euclid Collaboration: Moneti et al. 2022) and available radio data in the fit, nor does it consider AGN templates, which are relevant to the present work. This is also the reason why we did not include information on host galaxy masses in our analysis, since for consistency with the adopted redshifts we would have had to estimate them from B25, but those results are not yet available.

The 144 MHz radio luminosities for the B25 sample were then derived for the adopted cosmology and Bayesian redshifts by assuming an average radio spectral slope of $\alpha = 0.7$ independent of redshift, which holds with a good approximation for the overwhelming majority of relatively low-luminosity radio sources – both AGNs and SFGs (e.g. Magliocchetti et al. 2016; Toba et al. 2019; Calistro Rivera et al. 2017). We note that considering a spectral slope of 0.67 or 0.73, as derived by Calistro Rivera et al. (2017) for AGNs and SFGs separately, would produce a change in radio luminosity of less than 6%. The radio luminosity distribution as a function of redshift for the B25 sample is presented in the left-hand panel of Fig. A.1.

2.2. Active Galactic Nucleus or star-forming galaxy?

A tricky step in the process of identifying extragalactic sources observed in monochromatic radio surveys is distinguishing between the radio emission of AGN origin and that due to star-forming processes (e.g. Smolčić et al. 2017; Whittam et al. 2022; Best et al. 2023). In the local Universe, things are rather straightforward, since the majority of radio-loud sources are associated with massive elliptical galaxies with little or no ongoing star-formation activity (for a more refined analysis of the local population of hosts, see, e.g. Janssen et al. 2012). They are generally 'red and dead', present radio-to-optical flux ratios[1] larger than 30, and show a remarkable tightness in the K-band magnitude versus redshift relation, at least out to $z \simeq 1$ (e.g. Lilly & Longair 1984; Best et al. 2005; Capetti et al. 2022). On the other hand, SFGs present a very tight correlation between their far-IR and radio luminosities (e.g. Delhaize et al. 2017; Calistro Rivera et al. 2017), supposedly due to the presence of massive stars, which on the one hand heat dust, therefore producing IR emission, and on the other hand generate supernova events that accelerate cosmic rays and thus produce radio-synchrotron radiation (e.g. Condon 1992). However, at high redshifts, discerning between these two populations becomes more uncertain (see Magliocchetti 2022 for a review). This is why in this work, as in previous ones (Magliocchetti et al. 2016, 2017,

[1] Defined as $q_R = F_{1.4\,\mathrm{GHz}}\,10^{(R-12.5)/2.5}$, where F is expressed in millijanskys and R is the R-band magnitude.

Table 1. Properties of the radio AGN sample.

	AGN	Matched	Mer (optical)	Non-Mer (optical)	S (radio)	E (radio)	S+ Mer	S+ Non-Mer	E+ Mer	E+ Non-Mer
$0.5 < z < 2$	1793	819	308	201	667	152	239	180	69	21
$0.5 < z < 1$	870	521	214	125	413	108	162	112	52	13
$1 < z < 2$	923	298	94	76	254	44	77	68	17	8
$P < 10^{24}$ & $0.5 < z < 2$	1086	554	194	154	522	32	183	149	11	5
$P > 10^{24}$ & $0.5 < z < 2$	707	265	114	47	145	120	56	31	58	16
$10^{23.35} < P < 10^{24.2}$ and $0.5 < z < 1$	453	260	96	67	213	47	78	60	18	7
$10^{23.35} < P < 10^{24.2}$ and $1 < z < 2$	511	171	52	47	170	1	51	47	1	0
$P > 10^{24.2}$ and $0.5 < z < 1$	126	83	46	9	24	59	13	3	33	6
$P > 10^{24.2}$ and $1 < z < 2$	412	127	42	29	84	43	26	21	16	8

Notes. The second column reports the number of all LOFAR AGNs obtained from the work of B25, the third the number of those that are also present in the catalogue of EC:LM26, the fourth the number of radio AGNs with optical counterparts classified as mergers (Mer), and the fifth the radio AGNs with optical counterparts classified as non-interacting galaxies (Non-Mer). The sixth column provides the number of LOFAR AGNs with a compact radio morphology (S), and the seventh shows the number of those that instead show extended radio morphologies (E). Finally, columns 8–11 present the number of radio AGNs with combined cases of radio and optical morphologies. Different rows are for various redshift and 144 MHz radio-luminosity (P) cuts expressed in W Hz^{-1} sr^{-1}, as indicated in the first column.

Table 2. Properties of the radio SFG sample.

	SFG	Matched	Mer (optical)	Non-Mer (optical)	S (radio)	E (radio)	S+ Mer	S+ Non-Mer	E+ Mer	E+ Non-Mer
$0.5 < z < 2$	9299	3679	865	1510	3678	1	865	1510	0	0
$0.5 < z < 1$	4275	2455	570	1110	2454	1	570	1110	0	0
$1 < z < 2$	5024	1224	295	400	1224	0	295	400	0	0
$P < 10^{23}$ & $0.5 < z < 2$	3473	1985	442	918	1985	0	442	918	0	0
$P > 10^{23}$ & $0.5 < z < 2$	5826	1694	423	592	1693	1	423	592	0	0
$10^{22.7} < P < 10^{23}$ and $0.5 < z < 1$	1844	1061	255	464	1061	0	255	464	0	0
$10^{22.7} < P < 10^{23.3}$ and $1 < z < 2$	1417	554	120	207	554	0	120	207	0	0
$P > 10^{23}$ and $0.5 < z < 1$	968	561	149	219	560	1	149	219	0	0
$P > 10^{23.3}$ and $1 < z < 2$	3607	670	175	193	670	0	175	193	0	0

Notes. As in Table 1, but for the sub-population of radio-selected SFGs.

2018, 2020), we decided to rely on the method introduced in Magliocchetti et al. (2014).

The approach is based on the work of McAlpine et al. (2013), which provided luminosity functions at 1.4 GHz (hereafter RLF) separately for the two classes of AGNs and SFGs up to redshifts of $z \simeq 2.5$. Their results show that the 1.4 GHz radio luminosity, $P_{\rm cross}$, beyond which AGN-powered galaxies become the dominant radio population scales with redshift roughly as

$$\log_{10}\left[P_{\rm cross}(z)/P_{0,\rm cross}\right] = z \qquad (1)$$

up to $z \sim 1.8$; it then remains constant to $P_{\rm cross} \simeq 10^{23.5}$ W Hz^{-1} sr^{-1} at least up to $z \simeq 2.5$. The value $P_{0,\rm cross} = 10^{21.7}$ W Hz^{-1} sr^{-1} is what is found in the local Universe and roughly coincides with the break in the radio luminosity function of SFGs (cf. Magliocchetti et al. 2002; Mauch & Sadler 2007). Beyond this luminosity, the RLF of SFGs steeply declines, and the contribution of this population to the total radio counts is drastically reduced to a negligible percentage. The same trend is true at higher redshifts, and given the steepness of the RLF of SFGs (as opposed to the flatter trend of AGNs at all z), the adopted method – which selects all sources with radio luminosities beyond the time-evolving $P_{\rm cross}$ as radio AGNs – has the important advantage of producing a clean sample (e.g. in the first 0.1 dex in $P_{1.4\,\rm GHz}$ beyond $P_{\rm cross}$, the contamination from SFGs is already a mere 20%, and it rapidly becomes negligible at higher radio luminosities; cf. Magliocchetti et al. 2016), while only necessitating redshift determinations instead of expensive spectroscopy or multi-wavelength information for the sources being considered.

In order to proceed with the above method, we then rescaled the LOFAR luminosities to 1.4 GHz by assuming an average radio spectral index of $\alpha = 0.7$ (see Sect. 2.1). We then distinguished between radio emission from AGNs and SFGs by means of Eq. (1) for $z \leq 1.8$ and by fixing $P_{\rm cross}(z) = 10^{23.5}$ W Hz^{-1} sr^{-1} at higher redshifts. This procedure identified 4011 AGNs (3946 if using the redshifts derived with the minimum χ^2 method, cf. B25) and 15 390 sources classified as SFGs (15 455 if using redshifts derived with the minimum χ^2 method). We stress here (cf. Magliocchetti 2022) that, while the AGN selection is clean and subject to very little contamination from the population of SFGs, this is not true for the latter class since SFGs selected as in Eq. (1) are a mixed bag of all those sources that emit in the radio band as a result of processes connected to star formation. These include genuine SFGs as well as radio-quiet AGNs whose host galaxies are actively forming stars (e.g. Padovani 2016). Contamination from low-power radio AGNs (i.e. radio emission of AGN origin, as opposed to that of radio-quiet AGNs, which is

due to star-forming processes within the galaxy) is instead of a much lower level and rapidly decreases with decreasing radio luminosity for the same reasons discussed regarding the selection of the radio-AGN sample (cf. McAlpine et al. 2013 and Magliocchetti et al. 2016).

Indeed, the fraction of radio-emitting AGNs obtained as in Eq. (1) is remarkably similar to the ∼18% derived by Best et al. (2023) on the other three LOFAR deep fields once their LERGs and HERGs were combined, since our method is agnostic to this distinction. That of SFGs is instead higher (∼81% versus the ∼68% of Best et al. 2023). However, as expected from the above discussion, this discrepancy is largely reduced if we add the SFGs and the ∼9% contribution from radio-quiet AGNs to the Best et al. (2023) sample. We attribute the remaining ∼4% discrepancy to contamination from low-power radio AGNs in our SFG sample.

In spite of the mixed nature of the star-forming sample (∼85% *bona fide* SFGs and ∼11% radio-quiet AGNs according to Best et al. 2023), since interesting information can also be obtained for these objects, in the following we continue to label them with the cumulative name of SFGs and proceed with their analysis, warning the reader to keep the above caveat in mind.

As a final step, for the creation of our master catalogue, we removed 1045 objects (5% of the original sample) that had a different classification when using Bayesian versus minimum χ^2 redshifts from the AGNs and star-forming samples obtained as in Eq. (1). This was done to ensure that all the sources with dubious redshift determinations were excluded. Indeed, since the adopted selection method only depends on redshift once the radio flux is given, different classifications for a single object imply a large discrepancy between photometric redshifts derived with the two different approaches.

After this final cleaning, we were left with 14 900 SFGs (3340 with spectroscopic redshifts) and 3456 AGNs (647 with spectroscopic redshifts), 438 (i.e. ∼13%) of which have an extended morphology. This is only true for 26 SFGs (corresponding to 0.17% of the parent sample), and provides a reassuring check for the adopted classification criterion, since we do not expect processes associated with star formation to produce extended radio morphologies. We note that in principle the adoption of the full probability distribution functions (pdfs) for the photometric redshifts might have an effect on some classifications as such pdf distributions can be broad (e.g. Hale et al. in preparation). However, given the cleaning procedures explained above, and the fact that many (especially $z < 1$) sources are endowed with spectroscopic redshifts, we do not expect this effect to introduce appreciable variations into our samples.

The redshift distributions of both AGNs and SFGs in the $0.5 < z < 2$ redshift range relevant to the following analysis (see Sect. 3) are shown in the middle and right-hand panels of Fig. 1, while their luminosity distributions in the same redshift range are provided in the middle and right-hand panels of Fig. 2. The left-hand panels of both figures show the reproductions of the redshift and luminosity distributions of the parent radio sample. The middle panels of Figs. 1 and 2 additionally present the trends for the sub-population of extended radio AGNs. It can be seen that their redshift distribution closely follows that of the whole radio AGN population, while – as expected – their radio luminosities are shifted towards the bright end of the distribution.

3. The combined catalogue

For the following analysis, we made use of the catalogue presented by EC:LM26. In brief, the authors provided the first classification of *Euclid* galaxies divided into mergers versus non-mergers or non-interacting galaxies based on their VIS images in the *Euclid* Deep Fields. The work processed observations in the VIS/I_E band with a convolutional neural network (CNN) trained on cosmological hydrodynamical simulations to classify galaxies as mergers and non-mergers, where the merger classification refers to major (stellar mass ratio of 1:4 or less) merging events. A redshift interval of $0.5 < z < 2$ was chosen to ensure that the adopted $8'' \times 8''$ thumbnail centred on each source corresponded to a roughly constant physical scale of 50 kpc × 50 kpc. Furthermore, in order to ensure as clean a catalogue as possible, EC:LM26 limited their analysis to galaxies with `DET_QUALITY_FLAG` < 4 to filter out contaminants, `SPURIOUS_FLAG` = 0 to exclude spurious sources, and `MUMAX_MINUS_MAG>-2.6` to filter out point-like sources. Finally, a cut at $I_E = 23.9 - 2.5 \log_{10}$(`FLUX_DETECTION_TOTAL`) = 23.5 was considered to exclude faint objects for which morphological classification was less robust given the depth of the survey and the resolution of the images. This procedure returned 941 730 galaxies, respectively recognised as mergers (∼18% of the parent sample), non-mergers (∼45% of the parent sample), and sources for which the classification was uncertain (the remaining ∼37%), according to the score of the classifier (≥0.59 for mergers, <0.35 for non-mergers, and between 0.35 and 0.59 for unclassified sources; see EC:LM26 for further information).

We then considered the positions of the optical counterparts of LOFAR sources from the work of B25 (see Sect. 2). These were matched to the catalogue provided by EC:LM26 by simply requiring offsets <0.″3. With this choice, chances for spurious associations are basically null. Within the redshift range of $0.5 < z < 2$ we have 1793 radio AGNs and 9299 SFGs. Of these, 819 AGNs (corresponding to ∼47% of the total) and 3679 SFGs (corresponding to ∼40%) are associated with an *Euclid* galaxy from the work of EC:LM26 (312 AGNs and 604 SFGs if only restricting to sources with a spectroscopic redshift determination). The properties of these two samples in the case of associations with galaxies classified by EC:LM26 as either merging or non-interacting systems are summarised in Tables 1 and 2. Unclassified systems are discussed in detail in Sect. 4.3. Regarding sources with a spectroscopic redshift determination, there are 186 SFGs associated with merging systems and 218 SFGs hosted by non-interacting galaxies (157 and 192 for $0.5 < z < 1$). There are instead 139 AGNs in merging systems and 63 AGNs in non-interacting galaxies (122 and 54 for $0.5 < z < 1$). Comparing the above numbers with those provided in Table 1 implies that about ∼52% of the $0.5 < z < 1$ AGNs in the matched and classified catalogue have a secure spectroscopic redshift determination.

The dashed histograms (dotted in the case of extended radio morphologies) in Fig. 1 illustrate the redshift distributions of the LOFAR sources in the matched catalogue. As can be seen from the bottom panels of the same figure, the fraction of radio sources with a counterpart from the EC:LM26 work is about ∼60%, which is approximately constant between $0.5 < z < 1$ in all the considered cases (whole population, radio AGNs including those with extended morphologies, and SFGs) and then presents a smooth decline between $z = 1$ and 2. As shown in the left panel of Fig. B.1, this is due to the $I_E = 23.5$ magnitude cut applied to the whole sample of VIS-selected *Euclid* galaxies (see above in this section). Indeed, we find that while below $z = 1$ ∼37.5% of *Euclid* galaxies are fainter than $I_E = 23.5$, this percentage increases to ∼85.7% at $z = 2$. We note that these values are in perfect agreement with those found in the case of LOFAR sources, independently of their classification (see Fig. 1). This

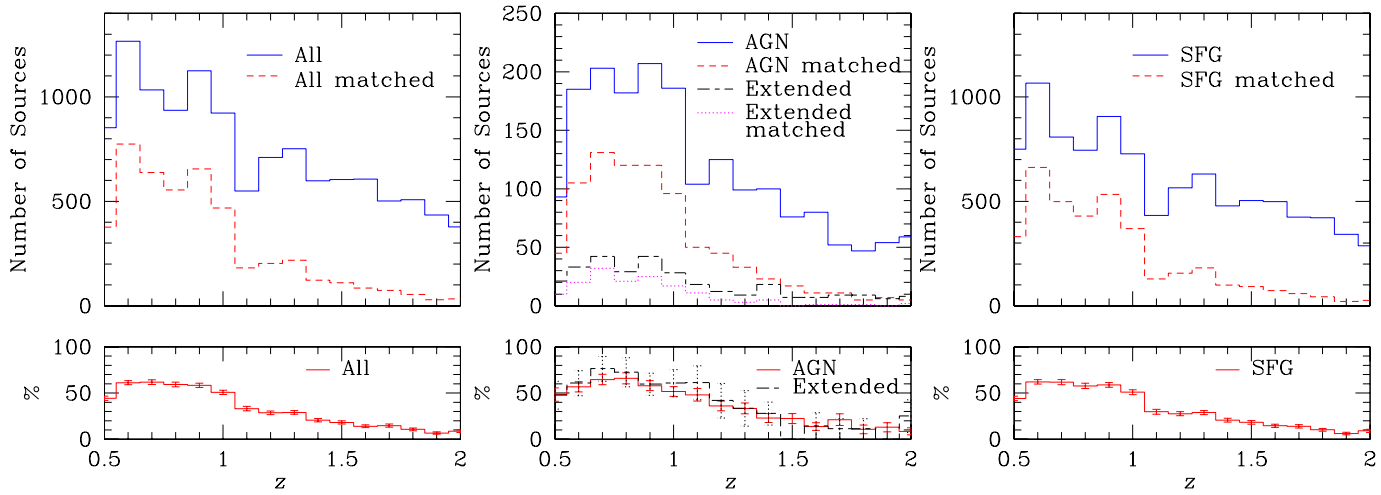

Fig. 1. Redshift distribution of LOFAR sources in the EDF-N region in the $0.5 < z < 2$ redshift interval. The left-hand panel refers to the whole sample, the middle panel to the sub-class of radio AGNs, and the right-hand panel to SFGs. In each top panel, the solid line refers to the parent radio sample from the work of B25, while the dashed histograms correspond to sources with optical counterparts from the work of EC:LM26. The bottom panels show the percentages obtained from the ratios between the above quantities, together with the associated (Poissonian) errors. The middle panel additionally presents the trends for AGNs with complex or extended radio morphology, short-long dashed lines for the parent sample and dotted lines for the matched sample.

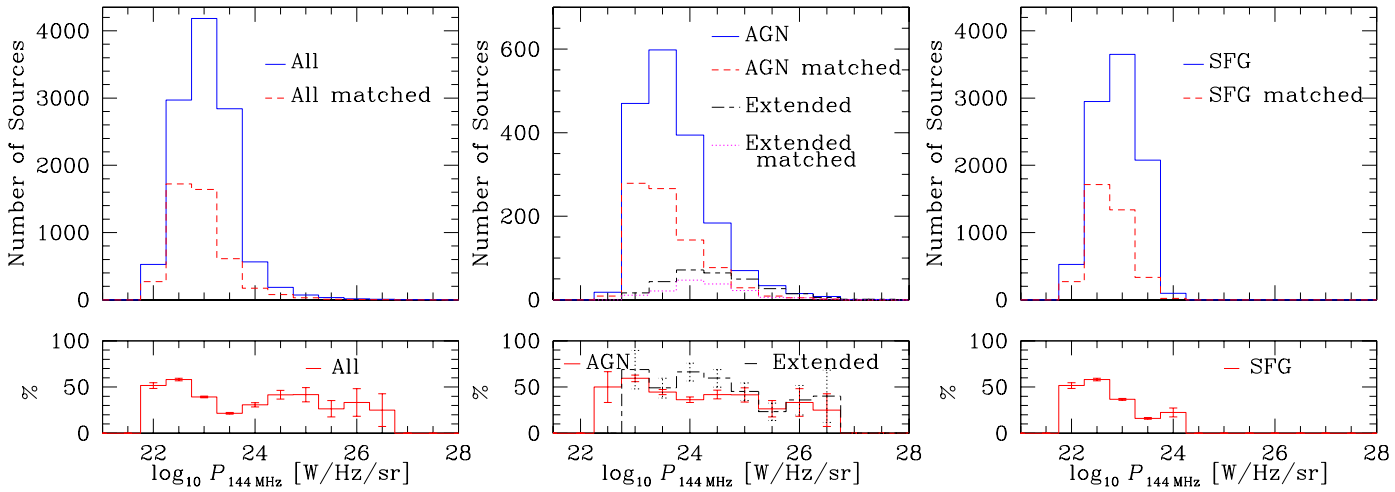

Fig. 2. Similar to Fig. 1, but for the 144 MHz luminosity distribution of LOFAR sources in the EDF-N belonging to the $0.5 < z < 2$ redshift interval.

implies an absence of redshift biases in our combined radio and optical sample.

Figure 2 instead shows the radio luminosity distribution of LOFAR sources belonging to the various sub-categories (all, radio AGNs, and SFGs) found within the $0.5 < z < 2$ range. Solid histograms (short-long dashed for extended radio morphologies) correspond to the parent radio sample obtained from the work of B25, while dashed histograms (dotted for extended radio morphologies) correspond to objects with a counterpart from the EC:LM26 work, regardless of the optical morphological classification of the host galaxy. The luminosity distribution of radio AGNs in the matched catalogue also closely follows that of the parent (AGN) sample in the case of AGNs with extended morphologies. As further shown in the bottom middle panel of Fig. 2, this implies that the matched radio AGN sample is free from radio luminosity biases, independently of the extension of radio emission. The same does not hold for the population of matched radio-selected SFGs, whose luminosity distribution presents a peak between $10^{21.5} < P_{144\,\mathrm{MHz}}/[\mathrm{W\,Hz^{-1}\,sr^{-1}}] < 10^{22.5}$ followed by a rather sharp decline at higher luminosities. The net result of the sum of these two trends (constancy of the fractional number of AGNs with radio luminosity and peaked distribution in the case of SFGs) is the behaviour observed in the left-hand panel of Fig. 2.

4. Results for radio AGNs and star-forming galaxies

In order to assess the relative role of mergers in the radio activity of galaxies, in Fig. 3 we show the fraction of radio-selected AGNs (left-hand panel) and SFGs (right-hand panel) respectively associated with non-interacting galaxies ('Non-Merging Systems') or galaxy–galaxy mergers ('Merging Systems'). The values plotted were obtained from those presented in Tables 1 and 2, and we also present a subdivision based on radio morphology for extended or compact emission. Note that the figure does not include LOFAR sources associated with *Euclid* galaxies that remained unclassified in the analysis of EC:LM26. A discussion on these objects is presented in Sect. 4.3.

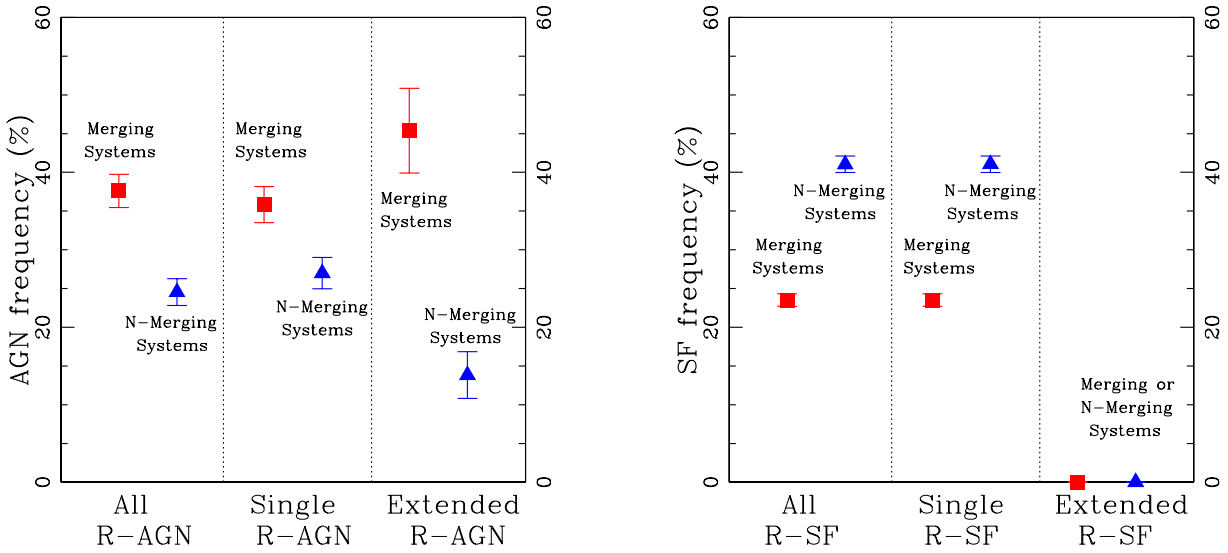

Fig. 3. Percentage of radio-selected AGNs (left-hand panel) and SFGs (right-hand panel) in the $0.5 < z < 2$ range associated with either non-interacting galaxies ('N-Merging Systems' – blue triangles) or galaxy–galaxy mergers ('Merging Systems' – red squares). Each panel is sub-divided into three sections, where the leftmost one shows the case for the whole sample of radio-selected AGNs or SFGs with a counterpart from the work of EC:LM26, the middle one is for radio sources with a compact radio structure, and the rightmost one is for objects presenting complex or extended radio morphologies. Error bars represent Poissonian uncertainties.

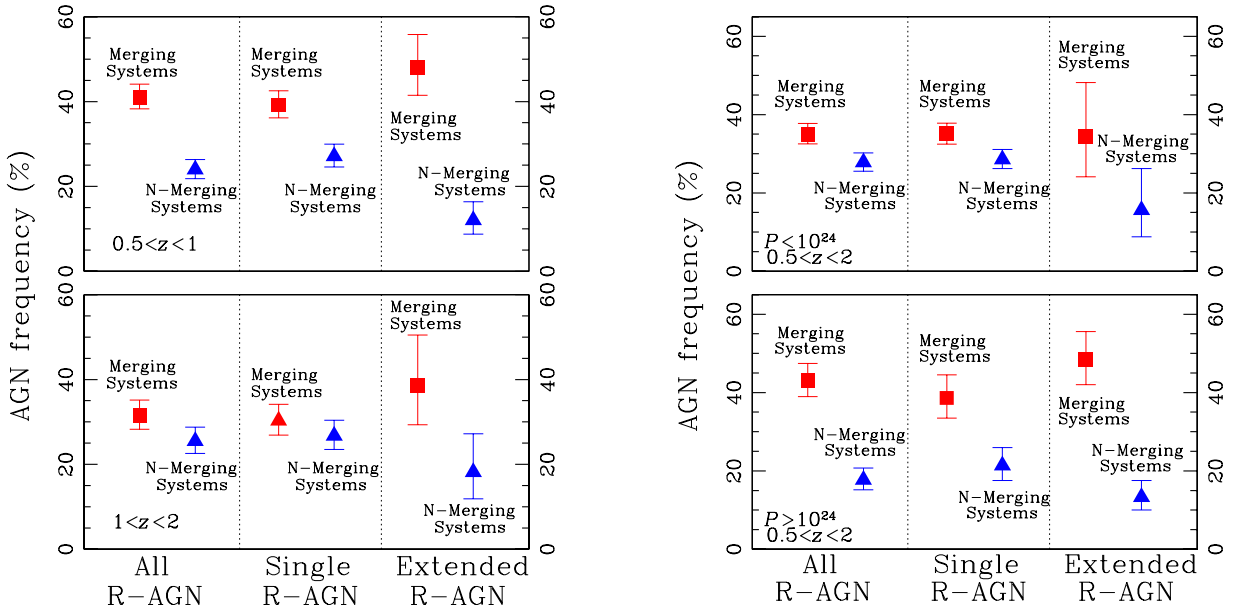

Fig. 4. Percentage of radio-selected AGNs associated with either non-interacting galaxies or galaxy–galaxy mergers. The sub-division of each panel and the colour and marker styles are as in Fig. 3. The left-hand panel presents the two cases for sources in the $0.5 < z < 1$ (top) and $1 < z < 2$ (bottom) ranges, while the right-hand panel shows objects of different radio luminosities, respectively $P_{144\,\mathrm{MHz}} <$ (top) and $>$ (bottom) 10^{24} W Hz^{-1} sr^{-1}, over the whole $0.5 < z < 2$ range. In this case, error bars represent Poissonian uncertainties derived according to Gehrels (1986).

A number of features can be appreciated here. The first and most striking one is the entirely opposite behaviour observed for radio-selected AGNs and SFGs. Indeed, regardless of their radio morphology (i.e. whether compact or extended), AGNs are preferentially associated with merging systems (~40% versus ~25% in non-mergers for the entire population of radio AGNs), while the opposite is true for SFGs (~25% versus ~40%). This clear preference of radio-selected AGNs to reside within merging systems becomes even more pronounced if we focus on those that present a complex or extended radio morphology. In this case, we note that about 50% of them are found to be associated with mergers, while only ~15% reside within non-interacting systems. Incidentally, we also note that the sample of SFGs with available optical morphological information does not contain any object with extended radio emission, so the values in the rightmost section of the right-hand panel are both zero. In the following, we analyse the cases for AGNs and SFGs separately.

4.1. Active Galactic Nuclei

The exquisite statistics provided by both LOFAR and *Euclid* observations of the EDF-N allow us to investigate the behaviour

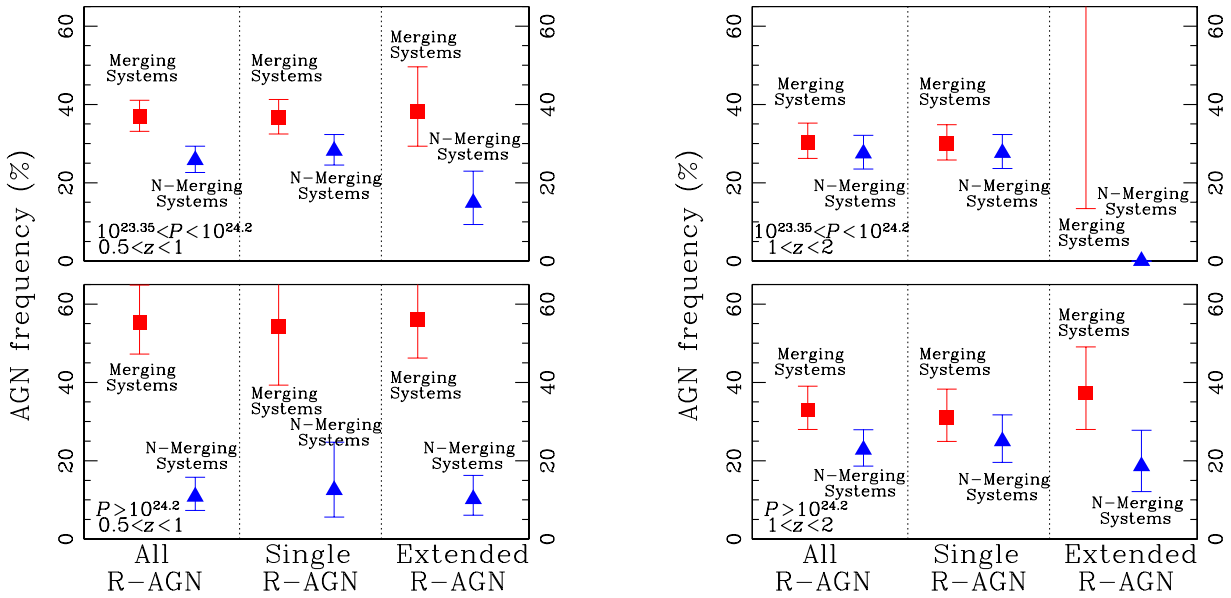

Fig. 5. Similar to Fig. 4, except that now different panels present different redshift and radio-luminosity (expressed in W Hz^{-1} sr^{-1} units) combinations (see text for details). The point in the top right part of the top right panel is off the scale and refers to one single object hosted by a merging system.

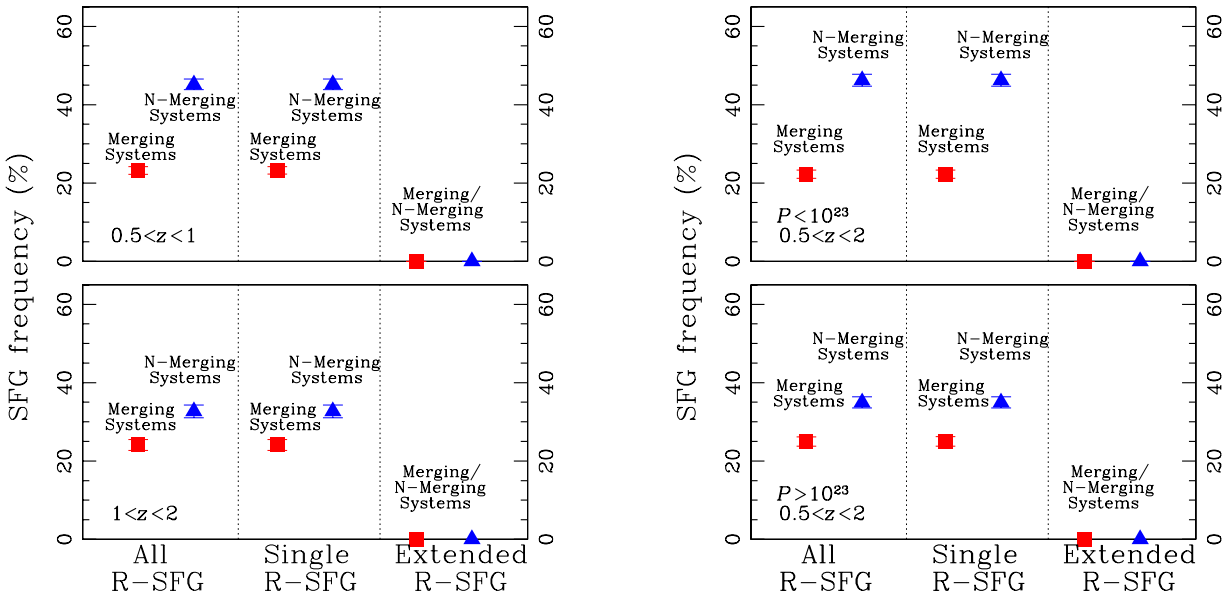

Fig. 6. Percentage of radio-selected SFGs associated with either non-merging galaxies or galaxy–galaxy mergers. The sub-division of each panel and the colour and marker styles are as in Fig. 3. The left-hand panel presents the two cases for sources in the $0.5 < z < 1$ (top) and $1 < z < 2$ (bottom) ranges, while the right-hand panel shows objects of different radio luminosities, respectively $P_{144\,\mathrm{MHz}}$ < (top) and > (bottom) 10^{23} W Hz^{-1} sr^{-1}, over the whole $0.5 < z < 2$ range. Error bars represent Poissonian uncertainties.

presented in Fig. 3 in greater detail as a function of redshift and radio luminosity in order to study possible evolutionary trends. In the case of radio AGNs this is done in the left-hand panel of Fig. 4 for redshift and the right-hand panel for radio luminosity. In all the considered cases (i.e. $0.5 < z < 1$, top-left; $1 < z < 2$, bottom-left; $P_{144\,\mathrm{MHz}} < 10^{24}$ W Hz^{-1} sr^{-1}, top-right; $P_{144\,\mathrm{MHz}} > 10^{24}$ W Hz^{-1} sr^{-1}, bottom right, where the latter two were obtained over the whole $0.5 < z < 2$ range), we note a preference for radio AGNs being associated with galaxy mergers. Furthermore, there is a more marked tendency observed for AGNs with extended radio morphologies, which are very seldom found within non-interacting galaxies. However, while such a behaviour is clearly evident in the case of relatively low redshift ($0.5 < z < 1$) or high luminosity ($P_{144\,\mathrm{MHz}} > 10^{24}$ W Hz^{-1} sr^{-1}) AGNs, this becomes less so for sources of relatively low radio luminosities ($P_{144\,\mathrm{MHz}} < 10^{24}$ W Hz^{-1} sr^{-1}) or redshifts in the range of $1 < z < 2$. Indeed, in the latter cases the small spread between the still higher fraction of radio AGNs hosted by merging systems and that of those residing within non-interacting galaxies is basically only driven by the subpopulation of complex or extended AGNs (see bottom-left and top-right panels of Fig. 4).

In order to disentangle redshift and radio-luminosity dependence and understand whether the observed trends are mainly

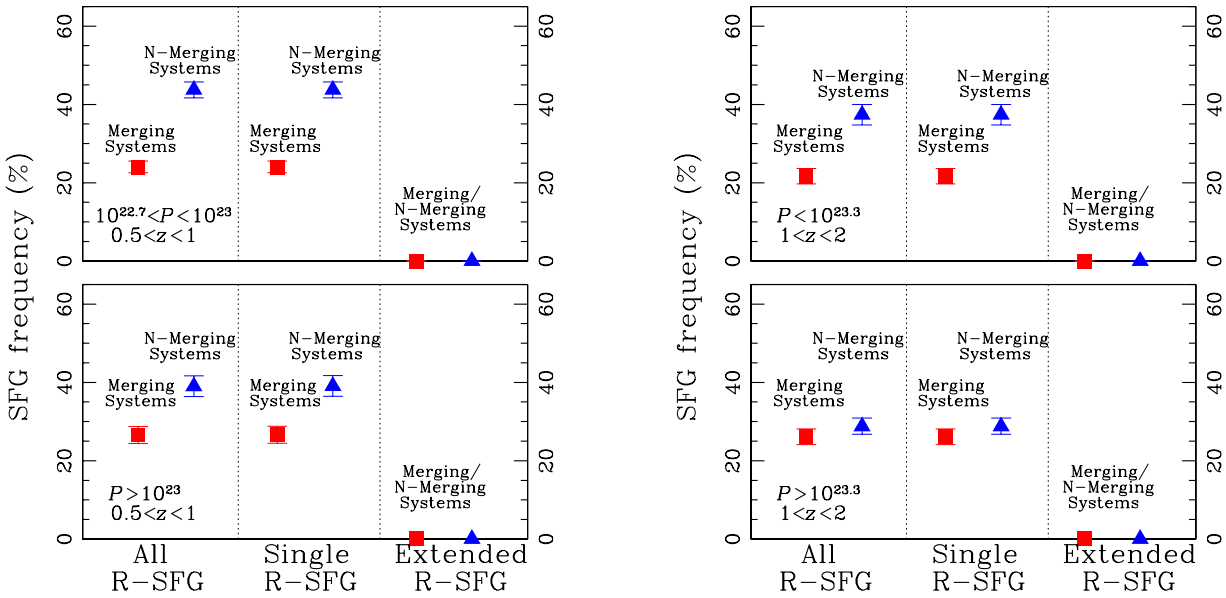

Fig. 7. Similar to Fig. 6, except that now different panels present different redshift and radio-luminosity (expressed in W Hz^{-1} sr^{-1}) combinations (see text for details).

due to evolutionary effects (i.e. vary with cosmic time) or are more connected with radio activity, we considered the following four subsets:

1. $0.5 < z < 1$; $10^{23.35} < P_{144\,\mathrm{MHz}}/[\mathrm{W\,Hz^{-1}\,sr^{-1}}] < 10^{24.2}$ (top-left panel of Fig. 5);
2. $1 < z < 2$; $10^{23.35} < P_{144\,\mathrm{MHz}}/[\mathrm{W\,Hz^{-1}\,sr^{-1}}] < 10^{24.2}$ (top-right panel of Fig. 5);
3. $0.5 < z < 1$; $P_{144\,\mathrm{MHz}}/[\mathrm{W\,Hz^{-1}\,sr^{-1}}] > 10^{24.2}$ (bottom-left panel of Fig. 5);
4. $1 < z < 2$; $P_{144\,\mathrm{MHz}}/[\mathrm{W\,Hz^{-1}\,sr^{-1}}] > 10^{24.2}$ (bottom-right panel of Fig. 5).

As in the previous case (see Fig. 4), we chose the redshift intervals to have a similar number of sources in the two low-z and high-z ranges and also to differentiate the regime where the redshift distribution of LOFAR sources with optical morphological information is independent of redshift from that where a dependence is instead observed (although merely driven by the optical $I_\mathrm{E} = 23.5$ cut; see Fig. 1 and Sect. 3). The radio-luminosity intervals were instead chosen to minimise possible incompleteness effects in the radio-luminosity distribution of LOFAR sources, while still allowing for a direct comparison between AGNs of similar brightnesses at high and low redshift. Indeed, as shown in Fig. A.1, in the $0.5 < z < 1$ range the AGN sample is complete above $P_{144\,\mathrm{MHz}} = 10^{23.35}\,\mathrm{W\,Hz^{-1}\,sr^{-1}}$, while between $z = 1$ and $z = 2$ this is only true above $P_{144\,\mathrm{MHz}} = 10^{24.2}\,\mathrm{W\,Hz^{-1}\,sr^{-1}}$.

Figure 5 presents the results of our analysis, where it should be kept in mind that all the panels are complete in radio luminosity except for the top-right one (low luminosities and high redshifts). It appears clear that the observed global trend of radio AGNs being preferentially hosted within merging systems (see left-hand panel of Fig. 3) is mainly driven by high-luminosity sources at low redshifts. Indeed, in this case we find that ∼56% of the radio AGNs considered are associated with merging systems, while a mere ∼10% are hosted by non-merging galaxies. Note that this result is roughly independent of the radio morphology of the sources. A smaller, but still significant, difference is observed in the low-luminosity and low-redshift regimes (top-left panel of Fig. 5), where this time the difference between the fractions of radio AGNs associated with merging versus non-merging systems is mainly due to AGNs that present extended radio morphologies. The situation changes at high redshifts, where we do not notice any significant preference for radio AGNs to appear within merging rather than non-merging systems and – if there is any hint (see bottom-right panel of Fig. 5) – this seems to be only driven by AGNs with complex or extended radio emission.

As discussed at greater length in Sect. 5, we interpret the observed behaviour of radio AGNs in the relatively local ($z < 1$) Universe through their need to accrete the gas necessary to trigger (radio) AGN activity from galaxy–galaxy encounters. This is even more necessary in the case of intense radio activity (i.e. high luminosities) and/or extended morphologies, where radio emission permeates most of the surrounding environment. Indeed, in the low-redshift Universe galaxies are more gas-deprived than their $z > 1$ counterparts (e.g. Genzel et al. 2015), so it seems that the main, if not the only (as in the case of bright AGNs with extended radio morphologies), way to accrete the gas that then triggers radio activity is via local encounters.

The situation appears different in the more distant Universe, since there does not seem to be any strong preference for radio AGN activity to happen in merging versus non-merging systems, apart from possibly in the case of extended radio morphologies. This is likely due to a higher abundance of available gas in the galaxies (e.g. Tacconi et al. 2010), which can be accreted by the AGNs even without the need to rely on close encounters such as mergers. However, in this latter case we recall that we might just be seeing the tip of the 'optically-bright AGN' iceberg since – as already discussed – due to the I_E magnitude cut (see Fig. B.1), only a small fraction (from about 30% at $z > 1$ to about 15% at $z \simeq 2$) of the general population of *Euclid* galaxies was considered in the analysis of EC:LM26 (and therefore in our work). Additionally, as recently shown by de Graaff et al. (2025), at higher redshifts the observed trends may be weaker than the true ones because the identification of mergers becomes harder.

4.2. Star-forming galaxies

An analysis very similar to that presented in Sect. 4.1 can be performed for the population of radio-emitting SFGs. This is

shown in Figs. 6 and 7. In more detail, Fig. 6 presents the fraction of SFGs associated with either a non-interacting or a merging system in the two redshift intervals $0.5 < z < 1$ (top left panel) and $1 < z < 2$ (bottom left panel) and – over the whole $0.5 < z < 2$ interval – in the two luminosity ranges, $P_{144\,\mathrm{MHz}} < 10^{23}\,\mathrm{W\,Hz^{-1}\,sr^{-1}}$ (top right panel) and $P_{144\,\mathrm{MHz}} > 10^{23}\,\mathrm{W\,Hz^{-1}\,sr^{-1}}$ (bottom right panel). What clearly emerges from investigation of the trends is a clear preference for SFGs to be hosted within non-interacting systems in all considered cases. However, we find that such a preference is more marked in the low-redshift regime and for low radio luminosities. Indeed, in both cases the percentage of SFGs associated with non-merging systems is as high as ∼45%. This may be a cosmic evolutionary effect (outer driver), or the observed trend could be due to different levels of the sources' radio activity (inner driver).

In order to conclude on the above point, in the same fashion as shown in Sect. 4.1, we sub-divided our sample into four intervals:

1. $0.5 < z < 1$; $10^{22.7} < P_{144\,\mathrm{MHz}}/[\mathrm{W\,Hz^{-1}\,sr^{-1}}] < 10^{23}$ (top-left panel of Fig. 7);
2. $1 < z < 2$; $10^{22.7} < P_{144\,\mathrm{MHz}}/[\mathrm{W\,Hz^{-1}\,sr^{-1}}] < 10^{23.3}$ (top-right panel of Fig. 7);
3. $0.5 < z < 1$; $P_{144\,\mathrm{MHz}}/[\mathrm{W\,Hz^{-1}\,sr^{-1}}] > 10^{23}$ (bottom-left panel of Fig. 7);
4. $1 < z < 2$; $P_{144\,\mathrm{MHz}}/[\mathrm{W\,Hz^{-1}\,sr^{-1}}] > 10^{23.3}$ (bottom-right panel of Fig. 7).

Here, all the radio luminosities are in $\mathrm{W\,Hz^{-1}\,sr^{-1}}$ units.

The choice for the redshift intervals follows the same argument presented in Sect. 4.1.

The radio luminosity intervals were instead chosen to minimise possible incompleteness effects in the radio-luminosity distribution. Indeed, as shown in Fig. A.1, in the $0.5 < z < 1$ range the SFG sample is complete above $P_{144\,\mathrm{MHz}} = 10^{22.7}\,\mathrm{W\,Hz^{-1}\,sr^{-1}}$, while between $z = 1$ and $z = 2$ this is only true above $P_{144\,\mathrm{MHz}} = 10^{23.3}\,\mathrm{W\,Hz^{-1}\,sr^{-1}}$. The $P_{144\,\mathrm{MHz}} = 10^{23}\,\mathrm{W\,Hz^{-1}\,sr^{-1}}$ cut in the low-redshift regime was instead chosen because no SFG is found above $P_{144\,\mathrm{MHz}} = 10^{23.3}\,\mathrm{W\,Hz^{-1}\,sr^{-1}}$.

Figure 7 presents the results of our analysis. As for the AGN case, all the panels are complete in radio luminosity except for the top right one (low luminosities and high redshifts). Low-luminosity SFGs clearly prefer to be hosted by non-merging systems. This is even more true in the low-redshift regime. Such a preference decreases to the point of vanishing at high redshifts for the radio-brighter sample. Interestingly, we notice that the fraction of SFGs associated with merging systems remains the same (∼20%) in all considered cases: it is the fraction of radio SFGs in non-interacting galaxies that varies, going from ∼45% for $0.5 < z < 1$ and $10^{22.7}\,\mathrm{W\,Hz^{-1}\,sr^{-1}} < P_{144\,\mathrm{MHz}} < 10^{23.3}\,\mathrm{W\,Hz^{-1}\,sr^{-1}}$ to ∼30% in the case of $1 < z < 2$ and $P_{144\,\mathrm{MHz}} > 10^{23.3}\,\mathrm{W\,Hz^{-1}\,sr^{-1}}$.

Given that the SFG sample is a mixed bag of pure SFGs and other low radio luminosity sources (see Sect. 2.2), it is unclear whether the observed trend of a stronger preference of faint radio SFGs to reside within non-merging systems is due to a real radio-luminosity effect (i.e. star-forming activity since these two quantities are intimately connected; see e.g. Condon 1992), in the sense that galaxies that are forming fewer stars are mostly non-interacting, or if there is a selection effect since the higher luminosity SFG sample is more contaminated not only by radio-quiet AGNs, but also by the low-luminosity tail of radio AGNs (Magliocchetti et al. 2002; McAlpine et al. 2013); the latter, as seen in Sect. 4.1, definitely prefer merging systems. Despite this uncertainty, the result that clearly emerges from our analysis is that – at variance with the radio-AGN case – radio-emitting SFGs are preferentially non-interacting galaxies. This implies that local encounters, especially at low redshifts (see left-hand panel of Fig. 7), are not the main source of gas availability or, in other words, that in the majority of cases reservoirs of gas already present within the galaxy suffice to fuel star formation.

4.3. Possible systematics

The present work has been subject to extensive tests for possible systematics that could hamper the significance of our results. We took into account radio-luminosity completeness effects (Sects. 4.1 and 4.2), removed all sources whose photometric redshifts were uncertain (Sect. 2.2), worked with an optical catalogue complete in I_E magnitude (Sect. 3 and Appendix B), and discussed possible contaminants in the sample of radio-selected SFGs. The next step was to further investigate systematics in the parent optical catalogue of EC:LM26.

Indeed, as described in Sect. 3, this work excludes all *Euclid* galaxies that show point-like structures in VIS imaging by construction. Since these objects are most likely non-interacting galaxies or quasars, their exclusion from the considered catalogue might introduce biases in our analysis. In order to test for this effect, in the right-hand panel of Fig. B.1 we plot the distribution of the values for the quantity `MUMAX_MINUS_MAG`, which characterises visual extension, for all *Euclid* galaxies with magnitudes of $I_\mathrm{E} \leq 23.5$ as a function of redshift. As it is possible to appreciate, only a handful of sources (those below the dashed line) were excluded from the EC:LM26 analysis, and this exclusion does not depend on redshift. In more detail, only 61 512 objects – corresponding to ∼5.7% of the parent optical sample – were discarded. It follows that even if we assume all these galaxies and quasars to be bona fide non-interacting systems, their addition to the analysis presented in the previous sections does not affect any of the results obtained.

As a further point, we had to consider all *Euclid* galaxies from EC:LM26 that have classifier scores between 0.35 and 0.59 and for this reason were considered dubious or unclassified cases (see Sect. 3). Extensive tests are presented in the above paper (see their Sect. 5.1) to assess the properties of these sources and their effect on the merger and non-mergers statistics, with the conclusion that they are an almost even mixture of merger and non-merger systems; as such, their addition is not expected to modify the results of either their study or ours. However, since the above tests were performed for the whole population of *Euclid* galaxies, while the present study concentrated on a subset of radio-detected sources for which different results might emerge (especially in the case of radio-selected AGNs), we also tackled this issue. In order to do so, we visually investigated the *Euclid* images for all 310 radio AGNs in our sample associated with an unclassified host. We were able to classify morphologies for 247 of them because some images were corrupted. In the case of compact radio AGNs, we find that 110 out of 198 (i.e. ∼56%) are associated with a non-interacting galaxy, while 88 (i.e. ∼44%) are associated with with a merging system. Concerning extended radio AGNs, we find that their hosts are evenly split into mergers and non-mergers (respectively, 24 mergers and 25 non-mergers). These results confirm what was found by EC:LM26 about the even mixture of merger and non-merger systems in unclassified cases, and we ultimately assessed the robustness of our analysis and conclusions.

Third, the impact of the classifier's imperfect performance on derived results was investigated by EC:LM26 using Monte Carlo simulations. These show variations of about six

percentage points for merging systems. It follows that our key findings remain qualitatively robust in spite of potential CNN misclassifications.

As a last point, we note that since AGNs and SFGs in our catalogue do not have inferred stellar masses (see Sect. 2.1), our analysis suffers from a lack of comparison with results from control samples. This might be relevant as there may be differences in mass between the AGN and the star-forming samples that could at least partially explain the observed difference in the merger fractions (e.g. Desmons et al. 2025). However, as discussed further on, our results for both the entire population of radio AGNs and SFGs are in excellent agreement with those obtained by EC:LM26, respectively, for their control-matched sample of AGNs selected at various wavelengths and for their control sample of non-active galaxies. Based on this evidence and the fact that our catalogue was compiled from that of EC:LM26, we expect the general conclusions of the present work to be robust.

5. Discussion

Thanks to the excellent statistics provided by both LOFAR and *Euclid*, we present the first large-scale study of the connection between radio emission and its morphology (i.e. compact versus complex or extended) in radio sources and the merging properties of their host galaxies. By dividing the radio sample into AGNs and SFGs, the data clearly indicate that radio AGNs prefer to reside within galaxies undergoing a merging event. This preference is more marked for AGNs that show signatures of complex or extended radio emission; indeed, about 50% of them are found to be associated with merging systems, while only ∼15% are hosted by a non-interacting galaxy. The observed trend is primarily driven by AGNs residing in the relatively local Universe ($z < 1$), especially in the case of high – $P_{144\,\mathrm{MHz}} > 10^{24}\,\mathrm{W\,Hz^{-1}\,sr^{-1}}$ – radio luminosities, for which we find ∼56% in merging systems versus ∼10% in non-mergers, regardless of radio morphology. This dichotomic behaviour is instead observed to disappear in the more distant Universe for redshifts $1 < z < 2$, where only bright AGNs with extended radio emission still seem to prefer merging systems.

The situation is totally reversed in the case of radio-emitting SFGs, which instead are mostly associated with non-interacting systems. This preference is more pronounced for low radio-luminosity and star-formation objects (∼40% versus ∼20% in mergers for $P_{144\,\mathrm{MHz}} < 10^{23}\,\mathrm{W\,Hz^{-1}\,sr^{-1}}$) regardless of redshift, but also in the case of brighter galaxies in the relatively local ($0.5 < z < 1$) Universe. Incidentally, we also note that the fraction of mergers in non-active galaxies reported by EC:LM26 – ∼18% in all considered cases – is remarkably similar to the ∼20% we find for our sample of radio-emitting SFGs at all luminosities and in all redshift intervals. This also provides us with a reassuring verification of the reliability of the results obtained for this population.

Selection effects (discussed in Sect. 4.3) aside, we interpret the above result as AGNs needing to accrete outer gas from local encounters in order to trigger (radio) activity, especially in the case of extended radio emission such as hot spots, lobes, and jets. This is mostly observed at $z < 1$, since in the local Universe galaxies are more gas deprived with respect to epochs approaching cosmic noon (e.g. Genzel et al. 2015), and an external supply might be needed to power radio emission of AGN origin (e.g. Heckman et al. 2024). Internal gas reservoirs instead seem sufficient to trigger star-formation within the majority of non-active galaxies, which indeed mostly appear as non-interacting systems at all redshifts, more so for moderate-to-low star-formation rates (see, e.g. Gürkan et al. 2018 for the conversion between 144 MHz radio luminosities and star-formation rates).

Results similar to ours for AGN candidates selected differently from radio emission are presented in EC:LM26. These authors considered four main categories: extragalactic point-like X-rays sources from 4XMM-DR13, CSC2, and eROSITA surveys (Euclid Collaboration: Roster et al. 2026); spectroscopically identified DESI QSOs (Siudek et al. 2024); AGN candidates detected via deep-learning-based image-decomposition methods (Euclid Collaboration: Margalef-Bentabol et al. 2026); and AGN candidates selected via their MIR colours (Assef et al. 2018).

Bearing in mind that their merger and non-merger fractions are defined in a way which is different from ours[2], and therefore have to be renormalised to be comparable with our results, we find that the percentage of radio AGNs associated with merging systems found in this work is in very good agreement with the values reported by EC:LM26. More specifically, they obtained around 40% (a little less for X-ray-selected AGNs) in all analysed cases, except for the AllWISE AGN sample with the lowest completeness level (∼26%; see Assef et al. 2018 for more details).

We stress that the above agreement holds for all radio AGNs considered in this work, regardless of their radio appearance, while – as already discussed at length – the fraction of radio AGNs with extended emission associated with merging systems is substantially higher, reaching values as high as 56%. This also implies that the fraction of extended radio AGNs associated with non-interacting galaxies is approximately halved (see Fig. 3). Putting all the information together, this implies that in order to have complex or extended radio emission, more close encounters are needed with respect to the case of unresolved AGN emission, regardless of the observed wavelength. The likely explanation for this can be found in the connection between availability of large amounts of gas and the ability of an AGN to produce radio emission that extends beyond the black hole neighbourhood.

One may question if the above result is only driven by radio morphology or if it hides an underlying dependence on the properties of gas accretion onto the central black hole (i.e. whether efficient or inefficient). As seen in the Introduction, efficient accretion is thought to produce the population of HERGs that present strong emission lines in their optical spectra and radiate at all wavelengths including the radio band. On the other hand, inefficient accretion – which only generates radio emission – is expected to produce the population of LERGs that present weak or no emission lines in their optical spectra (e.g. Best & Heckman 2012).

A thorough study of the populations of LERGs and HERGs would require investigation of the spectra for the LOFAR AGNs considered in this work, which unfortunately we do not yet have. However, we can still draw some conclusions by relying once again on radio morphology. Indeed, it is now assessed that there is an almost one-to-one correspondence between LERGs and FR I radio sources, in the sense that there are very few known examples of FR I HERGs (e.g. Mingo et al. 2019; Gürkan et al. 2021). On the other hand, FR IIs can come in both HERG and

[2] They considered $f_{\mathrm{merg/non\text{-}merg}} = \frac{N_{\mathrm{merger/non\text{-}merger}}}{N_{\mathrm{merger}}+N_{\mathrm{non\text{-}merger}}}$, while we adopted $f_{\mathrm{merg/non\text{-}merg}} = \frac{N_{\mathrm{merger/non\text{-}merger}}}{N_{\mathrm{TOT}}}$, which also takes into account the ∼36% of non-classified cases in the parent *Euclid* catalogue. Here, we call N_{merger} and $N_{\mathrm{non\text{-}merger}}$, respectively, the number of galaxies associated with a merging event or showing no interaction, while N_{TOT} denotes the total number of galaxies.

LERG types (e.g. Hine & Longair 1979; Chiaberge et al. 2000; Croston et al. 2018), with FR II LERGs being much more frequent at lower radio luminosities (e.g. Mingo et al. 2022).

With the aim of characterising our sample of radio AGNs, two members of our team visually investigated the LOFAR images of all 69 extended sources associated with merging systems independemtly (see Table 1). As can be seen in Figs. C.1 and C.2, where we show radio cutouts for a random selection of 48 of them, the AGNs with extended radio emission considered in this work are an even mixture of FR I and FR II morphologies. Furthermore, the work of Mingo et al. (2022) clearly shows that below $P_{144\,\mathrm{MHz}} \simeq 10^{25}\,\mathrm{W\,Hz^{-1}\,sr^{-1}}$ the contribution of HERGs to the FR II population is negligible. Our sample only includes a handful of sources brighter than the above limit. Based on both radio appearance and radio luminosity, we can safely conclude that the vast majority of our AGNs (including those with extended radio emission) are indeed LERGs.

The above discussion thus indicates that – at least within the population of LERGs – the observed enhanced frequency of galaxy mergers associated with extended radio emission of AGN origin is a result that only depends on radio morphology. Some combined LOFAR and *Euclid* images for FR I and FR II radio galaxies associated with merging systems are presented in Figs. C.3–C.4.

For completeness, in Fig. C.5 we also show LOFAR images for 20 out of the 21 extended radio AGNs hosted by non-interacting galaxies (see Table 1). As in the previous case, we also note that the sample consists of an even mixture of FR I and FR II morphologies. The only point worth mentioning is that three of the four most extended radio galaxies in our sample appear to be associated with non-merging systems. However, the statistics is too poor to draw any solid conclusion from this finding.

One last point to note is that the LOFAR images used in this work have a resolution of 6″. In the redshift range considered and for the adopted cosmology, this corresponds to physical scales between 36 kpc (at $z = 0.5$) and 50 kpc (at $z = 2$) and implies that the resolved radio emission we observe originates from the outskirts of a typical-sized galaxy and extends to larger scales. In the near future it will be interesting to compare the present results with those obtained using the LOFAR international stations, which allow us to zoom in on radio emission down to a resolution as high as 0.″3 (e.g., Morabito et al. 2025), capable to pierce right into the galaxy cores.

Acknowledgements. This work has made use of the *Euclid* Quick Release Q1 data from the *Euclid* mission of the European Space Agency (ESA), 2025, https://doi.org/10.57780/esa-2853f3b. The Euclid Consortium acknowledges the European Space Agency and a number of agencies and institutes that have supported the development of *Euclid*, in particular the Agenzia Spaziale Italiana, the Austrian Forschungsförderungsgesellschaft funded through BMK, the Belgian Science Policy, the Canadian Euclid Consortium, the Deutsches Zentrum für Luft- und Raumfahrt, the DTU Space and the Niels Bohr Institute in Denmark, the French Centre National d'Etudes Spatiales, the Fundação para a Ciência e a Tecnologia, the Hungarian Academy of Sciences, the Ministerio de Ciencia, Innovación y Universidades, the National Aeronautics and Space Administration, the National Astronomical Observatory of Japan, the Netherlandse Onderzoekschool Voor Astronomie, the Norwegian Space Agency, the Research Council of Finland, the Romanian Space Agency, the State Secretariat for Education, Research, and Innovation (SERI) at the Swiss Space Office (SSO), and the United Kingdom Space Agency. A complete and detailed list is available on the *Euclid* web site (www.euclid-ec.org). LB acknowledges support from the INAF Large Grant 'AGN & *Euclid*: a close entanglement' Ob. Fu. 01.05.23.01.14. Part of the research activities described in this paper were carried out with contribution of the Next Generation EU funds within the National Recovery and Resilience Plan (PNRR), Mission 4 – Education and Research, Component 2 – From Research to Business (M4C2), Investment Line 3.1 – Strengthening and creation of Research Infrastructures, Project IR0000034 – 'STILES – Strengthening the Italian Leadership in ELT and SKA'. MM, LB, MB, and IP acknowledge support from INAF under the Large Grant 2022 funding scheme (project 'Euclid and LOFAR Team up: a Unique Radio Window on Galaxy/AGN co-evolution').

References

Assef, R. J., Stern, D., Noirot, G., et al. 2018, ApJS, 234, 23
Best, P. N., & Heckman, T. M. 2012, MNRAS, 421, 1569
Best, P. N., Kauffmann, G., Heckman, T. M., et al. 2005, MNRAS, 362, 25
Best, P. N., Kondapally, R., Williams, W. L., et al. 2023, MNRAS, 523, 1729
Bichang'a, B., Kaviraj, S., Lazar, I., et al. 2024, MNRAS, 532, 613
Bickley, R. W., Ellison, S. L., Salvato, M., et al. 2024, MNRAS, 533, 3068
Bisigello, L., Giulietti, M., Prandoni, I., et al. 2025, Open J. Astrophys., 8, 101
Bondi, M., Scaramella, R., Zamorani, G., et al. 2024, A&A, 683, A179
Breiding, P., Chiaberge, M., Lambrides, E., et al. 2024, ApJ, 963, 91
Buat, V., Boquien, M., Małek, K., et al. 2018, A&A, 619, A135
Calistro Rivera, G., Williams, W. L., Hardcastle, M. J., et al. 2017, MNRAS, 469, 3468
Calistro Rivera, G., Alexander, D. M., Harrison, C. M., et al. 2024, A&A, 691, A191
Capetti, A., Brienza, M., Balmaverde, B., et al. 2022, A&A, 660, A93
Chiaberge, M., Capetti, A., & Celotti, A. 2000, A&A, 355, 873
Chiaberge, M., Gilli, R., Lotz, J. M., & Norman, C. 2015, ApJ, 806, 147
Comerford, J. M., Nevin, R., Negus, J., et al. 2024, ApJ, 963, 53
Condon, J. J. 1992, ARA&A, 30, 575
Croston, J. H., Ineson, J., & Hardcastle, M. J. 2018, MNRAS, 476, 1614
de Graaff, R., Margalef-Bentabol, B., Wang, L., et al. 2025, A&A, 697, A207
Delhaize, J., Smolčić, V., Delvecchio, I., et al. 2017, A&A, 602, A4
DESI Collaboration (Adame, A. G., et al.) 2024, AJ, 168, 58
Desmons, A., Brough, S., Lanusse, F., Canepa, L., & Khalid, A. 2025, MNRAS, 543, 2255
Duncan, K. J., Kondapally, R., Brown, M. J. I., et al. 2021, A&A, 648, A4
Ellison, S. L., Patton, D. R., & Hickox, R. C. 2015, MNRAS, 451, L35
Ellison, S. L., Viswanathan, A., Patton, D. R., et al. 2019, MNRAS, 487, 2491
Eróstegui, A., Mezcua, M., Siudek, M., Domínguez Sánchez, H., & Rodríguez Morales, V. 2025, A&A, 699, A330
Euclid Collaboration (Aussel, H., et al.) 2026, A&A, 711, A1 (Euclid Q1 SI)
Euclid Collaboration (Cropper, M., et al.) 2025, A&A, 697, A2
Euclid Collaboration (Huertas-Company, M., et al.) 2026, A&A, 711, A11 (Euclid Q1 SI)
Euclid Collaboration (La Marca, A., et al.) 2026, A&A, 711, A17 (Euclid Q1 SI)
Euclid Collaboration (Margalef-Bentabol, B., et al.) 2026, A&A, 711, A18 (Euclid Q1 SI)
Euclid Collaboration (Matamoro Zatarain, T., et al.) 2026, A&A, 711, A20 (Euclid Q1 SI)
Euclid Collaboration (McCracken, H. J., et al.) 2026, A&A, 711, A2 (Euclid Q1 SI)
Euclid Collaboration (Mellier, Y., et al.) 2025, A&A, 697, A1
Euclid Collaboration (Moneti, A., et al.) 2022, A&A, 658, A126
Euclid Collaboration (Quilley, L., et al.) 2026, A&A, 711, A8 (Euclid Q1 SI)
Euclid Collaboration (Roster, W., et al.) 2026, A&A, 711, A16 (Euclid Q1 SI)
Euclid Collaboration (Siudek, M., et al.) 2026, A&A, 711, A13 (Euclid Q1 SI)
Euclid Collaboration (Stevens, G., et al.) 2026, A&A, 711, A21 (Euclid Q1 SI)
Euclid Collaboration (Tucci, M., et al.) 2026, A&A, 711, A5 (Euclid Q1 SI)
Euclid Collaboration (Walmsley, M., et al.) 2026, A&A, 711, A9 (Euclid Q1 SI)
Euclid Quick Release Q1 2025, https://doi.org/10.57780/esa-2853f3b
Fanaroff, B. L., & Riley, J. M. 1974, MNRAS, 167, 31P
Gao, F., Wang, L., Pearson, W. J., et al. 2020, A&A, 637, A94
Gehrels, N. 1986, ApJ, 303, 336
Genzel, R., Tacconi, L. J., Lutz, D., et al. 2015, ApJ, 800, 20
Gordon, Y. A., Pimbblet, K. A., Kaviraj, S., et al. 2019, ApJ, 878, 88
Gürkan, G., Hardcastle, M. J., Smith, D. J. B., et al. 2018, MNRAS, 475, 3010
Gürkan, G., Croston, J., Hardcastle, M. J., et al. 2021, Galaxies, 10, 2
Hardcastle, M. J., & Croston, J. H. 2020, New Astron. Rev., 88, 101539
Heckman, T. M., Smith, E. P., Baum, S. A., et al. 1986, ApJ, 311, 526
Heckman, T. M., Roy, N., Best, P. N., & Kondapally, R. 2024, ApJ, 977, 125
Hickox, R. C., Jones, C., Forman, W. R., et al. 2009, ApJ, 696, 891
Hine, R. G., & Longair, M. S. 1979, MNRAS, 188, 111
Janssen, R. M. J., Röttgering, H. J. A., Best, P. N., & Brinchmann, J. 2012, A&A, 541, A62
Koulouridis, E., Gkini, A., & Drigga, E. 2024, A&A, 684, A111
La Marca, A., Margalef-Bentabol, B., Wang, L., et al. 2024, A&A, 690, A326
Lilly, S. J., & Longair, M. S. 1984, MNRAS, 211, 833
Magliocchetti, M. 2022, A&ARv, 30, 6
Magliocchetti, M., Maddox, S. J., Jackson, C. A., et al. 2002, MNRAS, 333, 100
Magliocchetti, M., Lutz, D., Rosario, D., et al. 2014, MNRAS, 442, 682
Magliocchetti, M., Lutz, D., Santini, P., et al. 2016, MNRAS, 456, 431

Magliocchetti, M., Popesso, P., Brusa, M., et al. 2017, MNRAS, 464, 3271
Magliocchetti, M., Popesso, P., Brusa, M., & Salvato, M. 2018, MNRAS, 473, 2493
Magliocchetti, M., Pentericci, L., Cirasuolo, M., et al. 2020, MNRAS, 493, 3838
Mauch, T., & Sadler, E. M. 2007, MNRAS, 375, 931
McAlpine, K., Jarvis, M. J., & Bonfield, D. G. 2013, MNRAS, 436, 1084
Mingo, B., Croston, J. H., Hardcastle, M. J., et al. 2019, MNRAS, 488, 2701
Mingo, B., Croston, J. H., Best, P. N., et al. 2022, MNRAS, 511, 3250
Morabito, L. K., Jackson, N., de Jong, J., et al. 2025, Ap&SS, 370, 19
Noll, S., Burgarella, D., Giovannoli, E., et al. 2009, A&A, 507, 1793
Padovani, P. 2016, A&ARev, 24, 13
Pierce, J. C. S., Tadhunter, C. N., Ramos Almeida, C., Bessiere, P. S., & Rose, M. 2019, MNRAS, 487, 5490
Pierce, J. C. S., Tadhunter, C. N., Gordon, Y., et al. 2022, MNRAS, 510, 1163
Pierce, J. C. S., Tadhunter, C., Ramos Almeida, C., et al. 2023, MNRAS, 522, 1736
Ramos Almeida, C., Tadhunter, C. N., Inskip, K. J., et al. 2011, MNRAS, 410, 1550
Ricci, C., Privon, G. C., Pfeifle, R. W., et al. 2021, MNRAS, 506, 5935
Sabater, J., Best, P. N., Hardcastle, M. J., et al. 2019, A&A, 622, A17
Schlafly, E. F., Meisner, A. M., & Green, G. M. 2019, ApJS, 240, 30
Siudek, M., Pucha, R., Mezcua, M., et al. 2024, A&A, 691, A308
Smolčić, V., Delvecchio, I., Zamorani, G., et al. 2017, A&A, 602, A2
Spinrad, H., Djorgovski, S., Marr, J., & Aguilar, L. 1985, PASP, 97, 932
Sutherland, W., & Saunders, W. 1992, MNRAS, 259, 413
Tacconi, L. J., Genzel, R., Neri, R., et al. 2010, Nature, 463, 781
Tadhunter, C. N., Morganti, R., di Serego Alighieri, S., Fosbury, R. A. E., & Danziger, I. J. 1993, MNRAS, 263, 999
Tanaka, M., Koike, M., Naito, S., et al. 2023, PASJ, 75, 986
Toba, Y., Yamashita, T., Nagao, T., et al. 2019, ApJS, 243, 15
van Haarlem, M. P., Wise, M. W., Gunst, A. W., et al. 2013, A&A, 556, A2
Villforth, C. 2023, Open J. Astrophys., 6, 34
Villforth, C., Herbst, H., Hamann, F., et al. 2019, MNRAS, 483, 2441
Wang, W., De Breuck, C., Wylezalek, D., et al. 2025, A&A, 696, A88
Whittam, I. H., Jarvis, M. J., Hale, C. L., et al. 2022, MNRAS, 516, 245

[1] INAF-Istituto di Astrofisica e Planetologia Spaziali, Via del Fosso del Cavaliere 100, 00100, Roma, Italy
[2] SRON Netherlands Institute for Space Research, Landleven 12, 9747 AD Groningen, The Netherlands
[3] Kapteyn Astronomical Institute, University of Groningen, PO Box 800, 9700 AV Groningen, The Netherlands
[4] INAF-Osservatorio Astronomico di Padova, Via dell'Osservatorio 5, 35122 Padova, Italy
[5] INAF, Istituto di Radioastronomia, Via Piero Gobetti 101, 40129 Bologna, Italy
[6] Department of Mathematics and Physics, Roma Tre University, Via della Vasca Navale 84, 00146 Rome, Italy
[7] INAF-Osservatorio Astronomico di Roma, Via Frascati 33, 00078 Monteporzio Catone, Italy
[8] School of Physics, HH Wills Physics Laboratory, University of Bristol, Tyndall Avenue, Bristol BS8 1TL, UK
[9] INFN-Sezione di Roma, Piazzale Aldo Moro, 2 – c/o Dipartimento di Fisica, Edificio G. Marconi, 00185, Roma, Italy
[10] Univ. Lille, CNRS, Centrale Lille, UMR 9189 CRIStAL, 59000 Lille, France
[11] Université Paris-Saclay, CNRS, Institut d'astrophysique spatiale, 91405 Orsay, France
[12] Leiden Observatory, Leiden University, Einsteinweg 55, 2333 CC Leiden, The Netherlands
[13] Department of Physics, Astronomy and Mathematics, University of Hertfordshire, College Lane, Hatfield AL10 9AB, UK
[14] Institute of Theoretical Astrophysics, University of Oslo, PO Box 1029 Blindern 0315, Oslo, Norway
[15] Department of Physical Sciences, Ritsumeikan University, Kusatsu, Shiga 525-8577, Japan
[16] Academia Sinica Institute of Astronomy and Astrophysics (ASIAA), 11F of ASMAB, No. 1, Section 4, Roosevelt Road, Taipei 10617, Taiwan
[17] Department of Physics, School of Advanced Science and Engineering, Faculty of Science and Engineering, Waseda University, 3-4-1 Okubo, Shinjuku, 169-8555 Tokyo, Japan
[18] Institute of Space Sciences (ICE, CSIC), Campus UAB, Carrer de Can Magrans s/n, 08193 Barcelona, Spain
[19] Institut d'Estudis Espacials de Catalunya (IEEC), Edifici RDIT, Campus UPC, 08860 Castelldefels, Barcelona, Spain
[20] INAF-Osservatorio di Astrofisica e Scienza dello Spazio di Bologna, Via Piero Gobetti 93/3, 40129 Bologna, Italy
[21] School of Physics & Astronomy, University of Southampton, Highfield Campus, Southampton SO17 1BJ, UK
[22] ESAC/ESA, Camino Bajo del Castillo s/n., Urb. Villafranca del Castillo, 28692 Villanueva de la Cañada, Madrid, Spain
[23] INAF-Osservatorio Astronomico di Brera, Via Brera 28, 20122 Milano, Italy
[24] IFPU, Institute for Fundamental Physics of the Universe, Via Beirut 2, 34151 Trieste, Italy
[25] INAF-Osservatorio Astronomico di Trieste, Via G. B. Tiepolo 11, 34143 Trieste, Italy
[26] INFN, Sezione di Trieste, Via Valerio 2, 34127 Trieste, TS, Italy
[27] SISSA, International School for Advanced Studies, Via Bonomea 265, 34136 Trieste, TS, Italy
[28] Dipartimento di Fisica e Astronomia, Università di Bologna, Via Gobetti 93/2, 40129 Bologna, Italy
[29] INFN-Sezione di Bologna, Viale Berti Pichat 6/2, 40127 Bologna, Italy
[30] Dipartimento di Fisica, Università di Genova, Via Dodecaneso 33, 16146 Genova, Italy
[31] INFN-Sezione di Genova, Via Dodecaneso 33, 16146 Genova, Italy
[32] Department of Physics "E. Pancini", University Federico II, Via Cinthia 6, 80126 Napoli, Italy
[33] INAF-Osservatorio Astronomico di Capodimonte, Via Moiariello 16, 80131 Napoli, Italy
[34] Instituto de Astrofísica e Ciências do Espaço, Universidade do Porto, CAUP, Rua das Estrelas, PT4150-762 Porto, Portugal
[35] Faculdade de Ciências da Universidade do Porto, Rua do Campo de Alegre, 4150-007 Porto, Portugal
[36] European Southern Observatory, Karl-Schwarzschild-Str. 2, 85748 Garching, Germany
[37] Dipartimento di Fisica, Università degli Studi di Torino, Via P. Giuria 1, 10125 Torino, Italy
[38] INFN-Sezione di Torino, Via P. Giuria 1, 10125 Torino, Italy
[39] INAF-Osservatorio Astrofisico di Torino, Via Osservatorio 20, 10025 Pino Torinese, TO, Italy
[40] European Space Agency/ESTEC, Keplerlaan 1, 2201 AZ Noordwijk, The Netherlands
[41] INAF-IASF Milano, Via Alfonso Corti 12, 20133 Milano, Italy
[42] Centro de Investigaciones Energéticas, Medioambientales y Tecnológicas (CIEMAT), Avenida Complutense 40, 28040, Madrid, Spain
[43] Port d'Informació Científica, Campus UAB, C. Albareda s/n, 08193 Bellaterra, Barcelona, Spain
[44] INFN section of Naples, Via Cinthia 6, 80126 Napoli, Italy
[45] Institute for Astronomy, University of Hawaii, 2680 Woodlawn Drive, Honolulu, HI 96822, USA
[46] Dipartimento di Fisica e Astronomia "Augusto Righi" – Alma Mater Studiorum Università di Bologna, Viale Berti Pichat 6/2, 40127 Bologna, Italy
[47] Instituto de Astrofísica de Canarias, Vía Láctea, 38205 La Laguna, Tenerife, Spain
[48] Institute for Astronomy, University of Edinburgh, Royal Observatory, Blackford Hill, Edinburgh EH9 3HJ, UK
[49] Jodrell Bank Centre for Astrophysics, Department of Physics and Astronomy, University of Manchester, Oxford Road, Manchester M13 9PL, UK
[50] European Space Agency/ESRIN, Largo Galileo Galilei 1, 00044 Frascati, Roma, Italy
[51] Université Claude Bernard Lyon 1, CNRS/IN2P3, IP2I Lyon, UMR 5822, Villeurbanne F-69100, France
[52] Aix-Marseille Université, CNRS, CNES, LAM, Marseille, France
[53] Institut de Ciències del Cosmos (ICCUB), Universitat de Barcelona (IEEC-UB), Martí i Franquès 1, 08028 Barcelona, Spain

[54] Institució Catalana de Recerca i Estudis Avançats (ICREA), Passeig de Lluís Companys 23, 08010 Barcelona, Spain
[55] Institut de Ciencies de l'Espai (IEEC-CSIC), Campus UAB, Carrer de Can Magrans s/n, Cerdanyola del Vallés, 08193 Barcelona, Spain
[56] UCB Lyon 1, CNRS/IN2P3, IUF, IP2I Lyon, 4 rue Enrico Fermi, 69622 Villeurbanne, France
[57] Mullard Space Science Laboratory, University College London, Holmbury St Mary, Dorking, Surrey RH5 6NT, UK
[58] Departamento de Física, Faculdade de Ciências, Universidade de Lisboa, Edifício C8, Campo Grande, PT1749-016 Lisboa, Portugal
[59] Instituto de Astrofísica e Ciências do Espaço, Faculdade de Ciências, Universidade de Lisboa, Campo Grande, 1749-016 Lisboa, Portugal
[60] Department of Astronomy, University of Geneva, ch. d'Ecogia 16, 1290 Versoix, Switzerland
[61] INFN-Padova, Via Marzolo 8, 35131 Padova, Italy
[62] Aix-Marseille Université, CNRS/IN2P3, CPPM, Marseille, France
[63] Space Science Data Center, Italian Space Agency, Via del Politecnico snc, 00133, Roma, Italy
[64] INFN-Bologna, Via Irnerio 46, 40126 Bologna, Italy
[65] University Observatory, LMU Faculty of Physics, Scheinerstrasse 1, 81679 Munich, Germany
[66] Max Planck Institute for Extraterrestrial Physics, Giessenbachstr. 1, 85748 Garching, Germany
[67] Universitäts-Sternwarte München, Fakultät für Physik, Ludwig-Maximilians-Universität München, Scheinerstrasse 1, 81679 München, Germany
[68] Jet Propulsion Laboratory, California Institute of Technology, 4800 Oak Grove Drive, Pasadena, CA 91109, USA
[69] Department of Physics, Lancaster University, Lancaster LA1 4YB, UK
[70] Felix Hormuth Engineering, Goethestr. 17, 69181 Leimen, Germany
[71] Technical University of Denmark, Elektrovej 327, 2800 Kgs. Lyngby, Denmark
[72] Cosmic Dawn Center (DAWN), Copenhagen, Denmark
[73] Max-Planck-Institut für Astronomie, Königstuhl 17, 69117 Heidelberg, Germany
[74] NASA Goddard Space Flight Center, Greenbelt, MD 20771, USA
[75] Department of Physics and Astronomy, University College London, Gower Street, London WC1E 6BT, UK
[76] Department of Physics and Helsinki Institute of Physics, University of Helsinki, Gustaf Hällströmin katu 2, 00014 Helsinki, Finland
[77] Department of Physics, University of Helsinki, PO Box 64, 00014 Helsinki, Finland
[78] Helsinki Institute of Physics, University of Helsinki, Gustaf Hällströmin katu 2, Helsinki 00014, Finland
[79] Laboratoire d'etude de l'Univers et des phenomenes eXtremes, Observatoire de Paris, Université PSL, Sorbonne Université, CNRS, 92190 Meudon, France
[80] SKAO, Jodrell Bank, Lower Withington, Macclesfield SK11 9FT, United Kingdom
[81] Centre de Calcul de l'IN2P3/CNRS, 21 avenue Pierre de Coubertin, 69627 Villeurbanne Cedex, France
[82] Dipartimento di Fisica "Aldo Pontremoli", Università degli Studi di Milano, Via Celoria 16, 20133 Milano, Italy
[83] INFN-Sezione di Milano, Via Celoria 16, 20133 Milano, Italy
[84] Universität Bonn, Argelander-Institut für Astronomie, Auf dem Hügel 71, 53121 Bonn, Germany
[85] Dipartimento di Fisica e Astronomia "Augusto Righi" – Alma Mater Studiorum Università di Bologna, Via Piero Gobetti 93/2, 40129 Bologna, Italy
[86] Department of Physics, Institute for Computational Cosmology, Durham University, South Road, Durham DH1 3LE, UK
[87] Université Paris Cité, CNRS, Astroparticule et Cosmologie, 75013 Paris, France
[88] CNRS-UCB International Research Laboratory, Centre Pierre Binétruy, IRL2007, CPB-IN2P3 Berkeley, USA
[89] Institut d'Astrophysique de Paris, 98bis Boulevard Arago, 75014 Paris, France
[90] Institut d'Astrophysique de Paris, UMR 7095, CNRS, and Sorbonne Université, 98 bis boulevard Arago, 75014 Paris, France
[91] Institute of Physics, Laboratory of Astrophysics, Ecole Polytechnique Fédérale de Lausanne (EPFL), Observatoire de Sauverny, 1290 Versoix, Switzerland
[92] Telespazio UK S.L. for European Space Agency (ESA), Camino bajo del Castillo s/n, Urbanizacion Villafranca del Castillo, Villanueva de la Cañada 28692, Madrid, Spain
[93] Institut de Física d'Altes Energies (IFAE), The Barcelona Institute of Science and Technology, Campus UAB, 08193 Bellaterra, Barcelona, Spain
[94] School of Mathematics and Physics, University of Surrey, Guildford, Surrey GU2 7XH, UK
[95] DARK, Niels Bohr Institute, University of Copenhagen, Jagtvej 155, 2200 Copenhagen, Denmark
[96] Waterloo Centre for Astrophysics, University of Waterloo, Waterloo, Ontario N2L 3G1, Canada
[97] Department of Physics and Astronomy, University of Waterloo, Waterloo, Ontario N2L 3G1, Canada
[98] Perimeter Institute for Theoretical Physics, Waterloo, Ontario N2L 2Y5, Canada
[99] Université Paris-Saclay, Université Paris Cité, CEA, CNRS, AIM, 91191 Gif-sur-Yvette, France
[100] Centre National d'Etudes Spatiales – Centre spatial de Toulouse, 18 avenue Edouard Belin, 31401 Toulouse Cedex 9, France
[101] Institute of Space Science, Str. Atomistilor, nr. 409 Măgurele, Ilfov 077125, Romania
[102] Dipartimento di Fisica e Astronomia "G. Galilei", Università di Padova, Via Marzolo 8, 35131 Padova, Italy
[103] Institut für Theoretische Physik, University of Heidelberg, Philosophenweg 16, 69120 Heidelberg, Germany
[104] Institut de Recherche en Astrophysique et Planétologie (IRAP), Université de Toulouse, CNRS, UPS, CNES, 14 Av. Edouard Belin, 31400 Toulouse, France
[105] Université St Joseph; Faculty of Sciences, Beirut, Lebanon
[106] Departamento de Física, FCFM, Universidad de Chile, Blanco Encalada 2008, Santiago, Chile
[107] Universität Innsbruck, Institut für Astro- und Teilchenphysik, Technikerstr. 25/8, 6020 Innsbruck, Austria
[108] Satlantis, University Science Park, Sede Bld, 48940 Leioa-Bilbao, Spain
[109] Instituto de Astrofísica e Ciências do Espaço, Faculdade de Ciências, Universidade de Lisboa, Tapada da Ajuda, 1349-018 Lisboa, Portugal
[110] Niels Bohr Institute, University of Copenhagen, Jagtvej 128, 2200 Copenhagen, Denmark
[111] Universidad Politécnica de Cartagena, Departamento de Electrónica y Tecnología de Computadoras, Plaza del Hospital 1, 30202 Cartagena, Spain
[112] Infrared Processing and Analysis Center, California Institute of Technology, Pasadena, CA 91125, USA
[113] Instituto de Astrofísica de Canarias (IAC); Departamento de Astrofísica, Universidad de La Laguna (ULL), 38200 La Laguna, Tenerife, Spain
[114] Université PSL, Observatoire de Paris, Sorbonne Université, CNRS, LERMA, 75014 Paris, France
[115] Université Paris-Cité, 5 Rue Thomas Mann, 75013 Paris, France
[116] ICL, Junia, Université Catholique de Lille, LITL, 59000 Lille, France

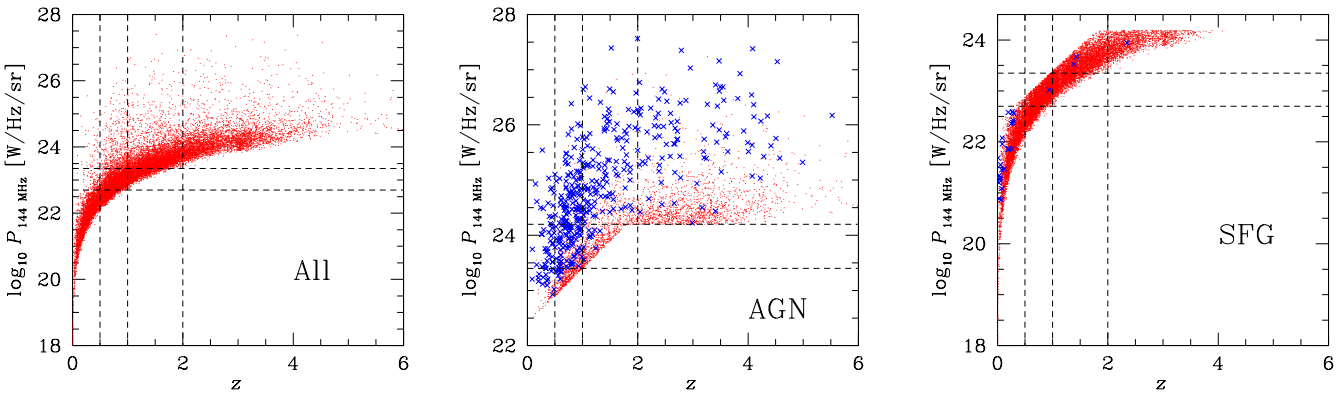

Fig. A.1. 144 MHz luminosity distribution of LOFAR sources in the EDF-N region as a function of redshift. The left-hand panel refers to the whole B25 sample, the middle panel to the sub-class of radio AGNs, and the right-hand panel to SFGs. The distinction between these two populations has been obtained via Eq. (1). Crosses indicate objects with an extended radio morphology. The horizontal dashed lines indicate the completeness limits of the whole (left-hand panel), AGN (middle panel), and SFG (right-hand panel) samples in the two redshift intervals $0.5 < z < 1$ and $1 < z < 2$ discussed in Sect. 4.

Appendix A: Radio luminosity distributions

We show here in Fig. A.1 the 144 MHz luminosities for radio-selected sources within the EDF-N.

Appendix B: Properties of the optical catalogue

In Fig. B.1 we show trends for all *Euclid* galaxies observed within the Q1 fields as a function of redshift.

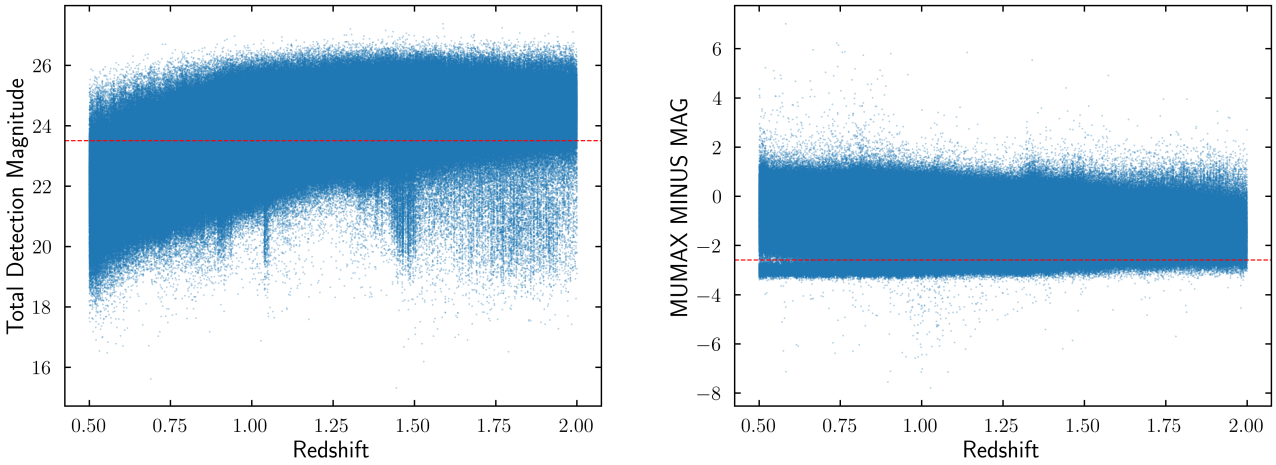

Fig. B.1. Left panel: Distribution of total detection magnitudes, I_E, for all *Euclid* galaxies in the range $0.5 < z < 2$. The dashed line indicates the cut at $I_E = 23.5$ applied by EC:LM26 for the production of their catalogue. Right panel: Distribution of values for the quantity `MUMAX_MINUS_MAG` which characterises the visual extension of *Euclid* galaxies. The dashed line represents the value of −2.6 adopted by EC:LM26 to exclude point-like sources.

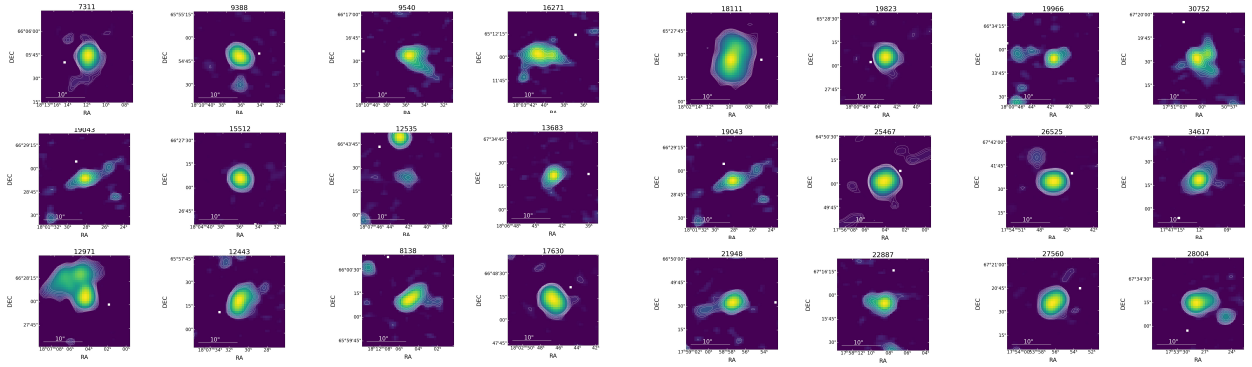

Fig. C.1. LOFAR images for a random selection of extended radio AGNs with FR I morphology.

Appendix C: Radio and optical images for AGNs with extended radio morphology

Here we show some LOFAR and *Euclid* images for complex or extended radio AGNs associated with either merging or non-merging galaxies (Figs. C.1 to C.5).

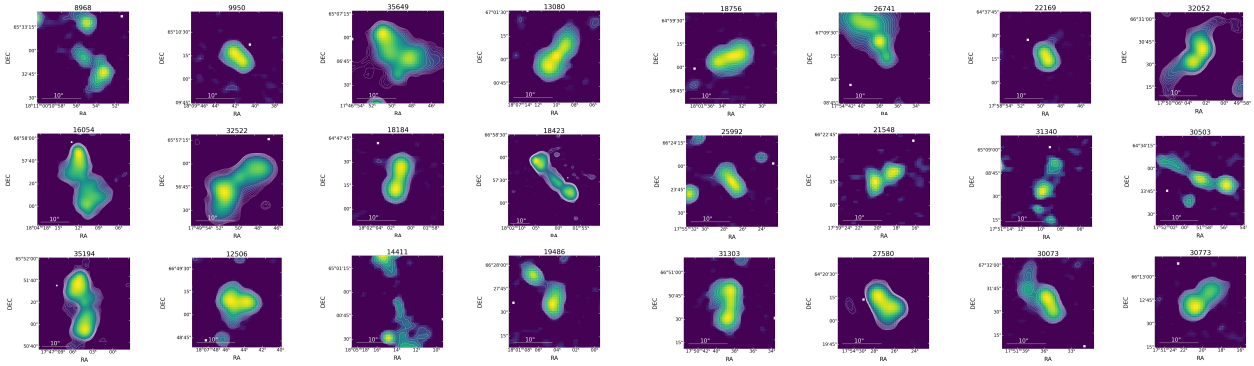

Fig. C.2. LOFAR images for a random selection of extended radio AGNs with FR II morphology.

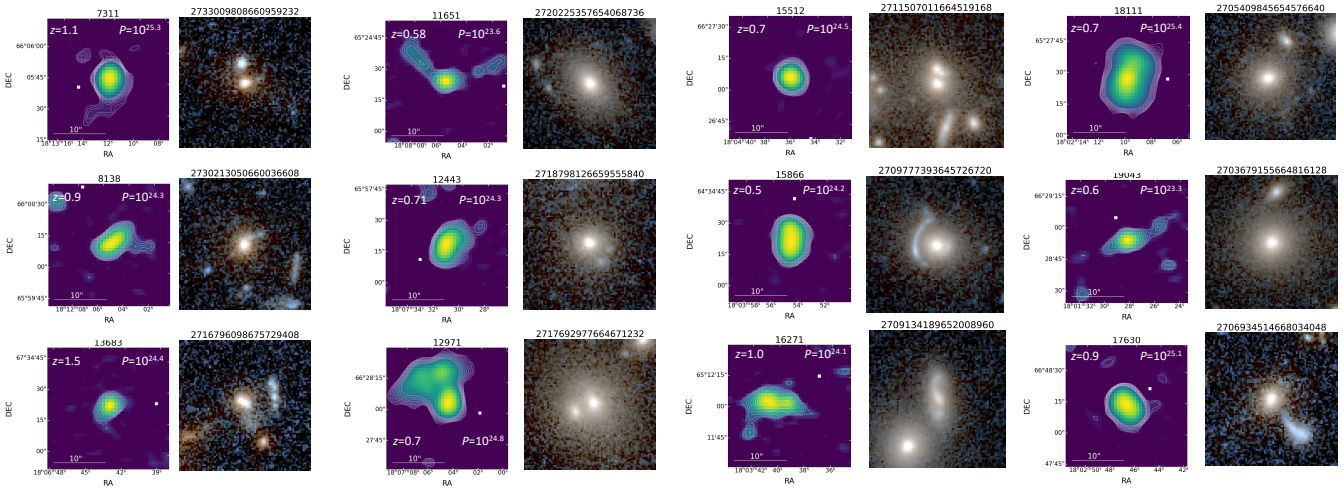

Fig. C.3. Some examples of LOFAR (left) and *Euclid* (right) images of AGNs with extended/FR I-like radio emission hosted by galaxies undergoing close encounters. Approximate redshifts and 144 MHz radio luminosities (in units W Hz^{-1} sr^{-1}) are also reported for all sources. The optical cutouts are 8″ × 8″, and the radio ones are as indicated. We choose different scales to be able to appreciate both the details of galaxy close encounters and the generally more extended radio emission.

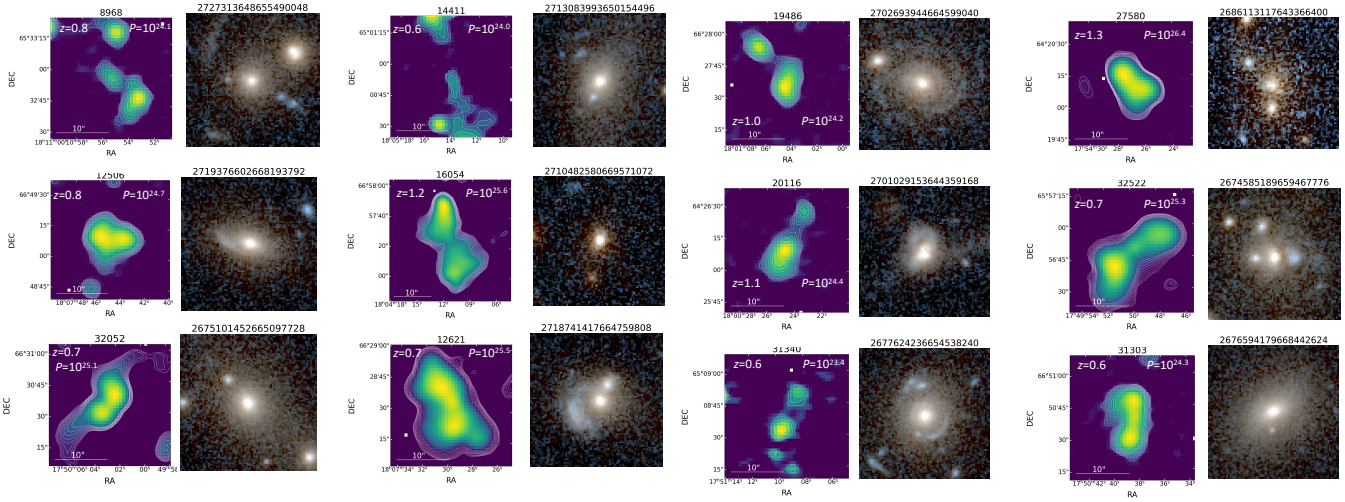

Fig. C.4. Some examples of LOFAR (left) and *Euclid* (right) images of AGNs with extended/FR II-like radio emission hosted by galaxies undergoing close encounters. Approximate redshifts and 144 MHz radio luminosities (in units W Hz^{-1} sr^{-1}) are also reported for all sources. The optical cutouts are 8″ × 8″, and the radio ones are as indicated. We choose different scales to be able to appreciate both the details of galaxy close encounters and the generally more extended radio emission.

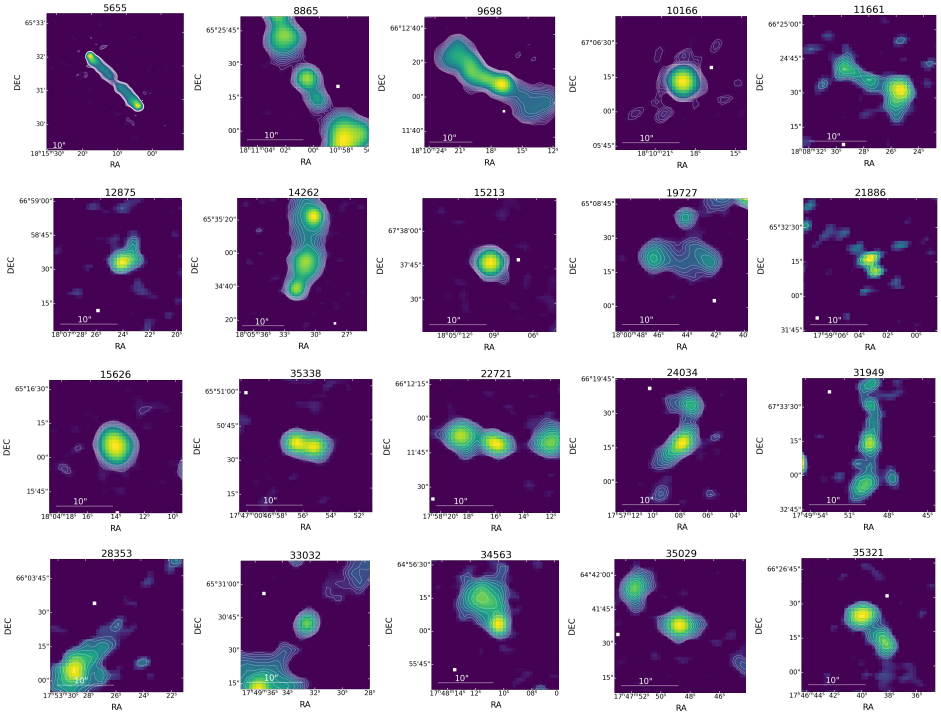

Fig. C.5. LOFAR images for 20 out of the 21 AGNs with extended radio emission hosted by non-merging systems (cf. Table 1).